NASA TECHNICAL NOTE

NASA TN D-2179

NASA TN D-2179

WIND-TUNNEL FLUTTER STUDIES OF THE SWEPTBACK T-TAIL OF A LARGE MULTIJET CARGO AIRPLANE AT MACH NUMBERS TO 0.90

by Charles L. Ruhlin, Maynard C. Sandford, and E. Carson Yates, Jr.

Langley Research Center
Langley Station, Hampton, Va.

NATIONAL AERONAUTICS AND SPACE ADMINISTRATION • WASHINGTON, D. C. • MARCH 1964

WIND-TUNNEL FLUTTER STUDIES OF THE SWEPTBACK T-TAIL OF A LARGE MULTIJET CARGO AIRPLANE AT MACH NUMBERS TO 0.90

By Charles L. Ruhlin, Maynard C. Sandford,
and E. Carson Yates, Jr.

Langley Research Center
Langley Station, Hampton, Va.

NATIONAL AERONAUTICS AND SPACE ADMINISTRATION

For sale by the Office of Technical Services, Department of Commerce,
Washington, D.C. 20230 -- Price $1.50

WIND-TUNNEL FLUTTER STUDIES OF THE SWEPTBACK T-TAIL OF A LARGE MULTIJET CARGO AIRPLANE AT MACH NUMBERS TO 0.90

By Charles L. Ruhlin, Maynard C. Sandford,
and E. Carson Yates, Jr.

SUMMARY

A flutter investigation of the T-tail of a currently projected multijet cargo airplane has been conducted in the Langley transonic dynamics tunnel at Mach numbers up to 0.90. The tail and aft fuselage of the model employed were geometrically, dynamically, and elastically scaled, whereas only the mass and stiffness characteristics of the forward fuselage, wings, and nacelles were simulated. This study included variations in flow density, stabilizer-pitch-actuator stiffness, fin-spar stiffness, roll and yaw stiffnesses of fin-stabilizer joint, rotational stiffnesses of elevators and rudder, stabilizer mass and yaw and roll inertias.

Within the ranges of the tests, no flutter occurred for the design configuration with control surfaces locked, with design elevator rotational stiffness, or with a simulated rudder-free condition. However, severe reductions in stabilizer-pitch-actuator stiffness or in elevator rotational stiffness did result in symmetric flutter. Increasing stabilizer mass and yaw and roll inertias by adding large weights to the stabilizer tips led to symmetric flutter which was studied over wide ranges of Mach number and flow density. Two antisymmetric flutter points were obtained for a configuration having stabilizer tip weights and a weaker-than-design fin spar.

INTRODUCTION

T-tails are being used with increasing frequency on airplanes which operate at high subsonic or transonic speeds. Such designs may offer several aerodynamic advantages over conventional tail configurations. (See ref. 1.) T-tails, however, are frequently subject to flutter instabilities because of inherent tendencies toward dynamic and aerodynamic coupling (refs. 2 to 7). Since theoretical methods for comprehensive T-tail flutter analyses have not yet reached a satisfactory level of reliability, extensive experimental flutter studies of each new T-tail design are usually required. (See refs. 8 and 9.)

This report contains the results of a wind-tunnel flutter investigation of the T-tail of a currently projected multijet cargo airplane. The tail and aft fuselage of the model employed were geometrically, dynamically, and elastically scaled. Although other portions of the model were not geometrically scaled, the

mass and elastic properties of the forward fuselage, wings, and nacelles were simulated in order to provide for any dynamic coupling between the tail and other portions of the airplane. Experiments were conducted in the Langley transonic dynamics tunnel in air at Mach numbers up to 0.65 and in Freon-12 at Mach numbers up to 0.90. (The design limit Mach number for the airplane is 0.89.) The model was tested on a mount system which permitted limited rigid-body motion in all six degrees of freedom. The investigation included variations in flow density, stabilizer-pitch-actuator stiffness, fin-spar stiffness, roll and yaw stiffnesses of fin-stabilizer joint, rotational stiffnesses of elevators and rudder, stabilizer mass and yaw and roll inertias.

SYMBOLS

A	amplitude of control-surface rotation about hinge axis, radians
A_{max}	maximum value of A, radians
EI	bending stiffness, lb-in.^{2}
f	flutter frequency, cps
f_e	natural frequency of elevator rotation, cps
f_r	natural frequency of rudder rotation, cps
f_θ	uncoupled pitch frequency of horizontal tail, cps
GJ	torsional stiffness, lb-in.^{2}
I_{ea}	mass moment of inertia of stabilizer section or fin section about its elastic axis, slug-ft^2
I_{hl}	mass moment of inertia of elevator or rudder about its hinge line, slug-ft^2
I_θ	mass moment of inertia of horizontal tail (including elevators, bullet fairing, and any additional weights) in pitch about horizontal-tail pivot axis, slug-ft^2
I_ψ	mass moment of inertia of horizontal tail (including elevators, bullet fairing, and any additional weights) in yaw about a vertical axis through intersection of fin elastic axis and stabilizer horizontal plane, slug-ft^2
I_ϕ	mass moment of inertia of horizontal tail (including elevator, bullet fairing, and any additional weights) in roll about intersection of stabilizer horizontal plane and plane of symmetry, slug-ft^2
M	Mach number

m_h total mass of horizontal tail (including elevator, bullet fairing, and any additional weights), slugs

m_v total mass of vertical tail (including rudder), slugs

q dynamic pressure, lb/sq ft

R gas constant, $ft^2/sec^2/^oR$

N_{Re} Reynolds number per foot

S_{ea} mass unbalance of stabilizer section or fin section about its elastic axis, slug-ft

S_{hl} mass unbalance of elevator or rudder about its hinge line, slug-ft

T static temperature, ^oR

V free-stream velocity, ft/sec

v volume of a conical frustum having horizontal-tail root chord as base diameter, horizontal-tail tip chord as upper diameter, and horizontal-tail semispan as height, 3.225 cu ft

γ ratio of specific heat at constant pressure to specific heat at constant volume

η_{ea} distance along elastic axis (spar center line) of fin or stabilizer measured from elastic-axis root, fraction of elastic-axis length

μ mass ratio of horizontal tail, $m_h/2\rho v$

ρ test-medium density, slugs/cu ft

Subscript:

o scaled design condition

Abbreviations:

BL buttock line, in.

FS fuselage station, in.

WL water line, in.

MODEL

General Description

A model of a currently projected multijet cargo airplane was used in this investigation. (See figs. 1 and 2.) The T-tail and aft fuselage of the model were geometrically, dynamically, and elastically scaled so that in Freon-12 Mach number, mass ratio, and reduced frequency were simulated for the airplane in the atmosphere; in air, only mass ratio and reduced frequency were correctly simulated. The mass and stiffness distributions of the forward fuselage, as well as the overall mass and elastic properties of the wings and nacelles, were also represented, although these components were not geometrically scaled. Specifically, the overall vibrational characteristics of the airplane wing with multiple engine pods were represented by a simulated wing with a single, simulated nacelle at the tip. The geometric properties given in table I are pertinent to all model configurations although several interchangeable structural members were employed in order to vary component stiffnesses.

Construction

Horizontal stabilizer.- The stabilizer was of a spar-and-pod type of construction (fig. 1(b)). A single rectangular box spar of welded magnesium alloy with one internal and one external flange welded on opposite sides of the spar provided the required stiffness distributions in bending and torsion. The pods, which contributed negligibly to stabilizer bending and torsional stiffnesses, were constructed of two pine bridge ribs and two balsa floating ribs covered with sheet balsa to form the airfoil contour. All pods were oriented perpendicular to the center line of the box spar (41 percent of streamwise chord) which was considered to be the stabilizer elastic axis. Each pod was covered with doped silk-span. Lead weights were installed in the pods to yield the required mass, center of gravity, and moment of inertia. The gaps between the pods were aerodynamically closed with sponge rubber.

The stabilizer was attached to the vertical tail by two aluminum bracket arms with ball bearing pivots which fitted on a lateral shaft mounted at the top of the fin spar (see fig. 1(d)). The stabilizer could be trimmed in pitch relative to the fin by means of a jack screw which was driven through an articulated shaft by an electric motor located in the fuselage. (See figs. 1(c) and 1(d).) The articulated shaft was connected to the stabilizer through a U-shaped metal spring which simulated the stiffness of the pitch-trim actuator.

Elevators.- The elevator spars were constructed of balsa covered with 0.015-inch-thick aluminum-alloy sheet. (See fig. 1(b).) The contour was built up of pine ribs covered with sheet balsa and doped silk-span.

The elevator hinge line was located at 75 percent of the stabilizer chord (streamwise). Two retaining ball bearings and four steel flexures were used to attach each elevator to the stabilizer. Each elevator was fully mass balanced by brass weights distributed along the leading edge. Left and right elevators

were flexibly interconnected in order to simulate the carry-through stiffnesses for both symmetric and antisymmetric modes.

Vertical fin.- The fin was of a spar-and-pod type of construction similar to that of the stabilizer (fig. 1(c)). The required bending and torsional stiffness distributions were provided by a single rectangular box-beam spar of welded magnesium alloy with an internal and an external flange on opposite sides of the box spar. The pods which formed the aerodynamic contour were constructed similarly to those of the stabilizer. All pods were oriented normal to the center line of the fin spar (40 percent of streamwise chord) which was considered to be the fin elastic axis. Lead ballast weights were installed in the pods to yield the required mass distribution.

The magnesium spar cap (fig. 1(c)), which provides a portion of the fin-stabilizer joint flexibility, is a bolted-on extension of the fin spar. A shaft projecting from each side of the spar cap engaged the bearings in the stabilizer support-bracket arms. (See fig. 1(d).) The fin-stabilizer joint area was enclosed by a bullet fairing which was constructed of balsa covered with doped silk. (See figs. 1(a) and 1(b).)

Rudder.- The rudder was constructed on a balsa spar covered with 0.010-inch-thick magnesium alloy. The contour was built up of pine ribs covered with balsa and doped Japanese tissue. The rudder rotated about 75 percent of the fin chord (streamwise) on two retaining ball bearings and three flexures. Except for a few of the initial tests, the rudder was not mass balanced. For the initial tests, 100-percent mass balance was obtained by taping small flat weights to the leading edge of the rudder.

For the final two tests, the rudder was removed and replaced by a fin extension built up of balsa ribs covered with balsa sheet and doped silk.

Fuselage.- The fuselage was of spar-and-pod construction. The major part of the fuselage (fig. 1(d)) was constructed of a 4-inch-square magnesium box spar with varying wall thickness (0.187 inch to 0.056 inch) to yield the required torsional stiffness distribution. Flanges of constant thickness but varying width were welded externally on all four sides of the spar to give the desired vertical and lateral bending stiffness distributions. The extreme aft-fuselage spar was constructed of a 4-inch circular aluminum tube of constant wall thickness with a tapered flange welded to the sides to obtain the desired stiffness distributions. The forward fuselage, which did not simulate the airplane geometrically, was composed of solid balsa pods which formed a cylinder around the spar. The geometrically scaled aft-fuselage pods were built of plywood bulkheads with magnesium inserts and were covered with sheet balsa (fig. 1(a)). Two rotating-unbalanced-mass shakers were mounted inside the nose of the fuselage spar in order to excite the vertical and lateral modes of the model.

Wings and nacelles.- Each simulated wing panel consisted of a solid, aluminum-alloy rectangular beam which was bolted onto an H-fitting mounted on the top of the fuselage spar. Balsa aerodynamic fairings were attached to the leading and trailing edges of the wing beams. (See figs. 1(a) and 1(d).) The simulated nacelles were constructed of an aluminum-alloy beam with a large lead

mass attached to the forward end to give the required mass properties. These nacelles were attached to the outboard ends of the wing beams by I-beam pylons which were streamlined with balsa fairings.

Mounting cage.- The mounting cage (figs. 1(a) and 1(d)) has four lengths of 0.20-inch-diameter music wire which are rigidly attached to the fuselage about the center of gravity and extended symmetrically above and below the center of gravity. At their extremities, these four vertical wires are attached to two exposed plates which are nominally parallel to the free stream. The upper plate was streamlined with balsa fairings. The model was supported in the tunnel by mounting cables which were attached to the two exposed plates of the mounting cage.

Instrumentation

Wire strain gages were mounted on the fin spar near the base and on the right and left sides of the stabilizer spar near the root. These gages were oriented to indicate deflections in bending and torsion. Small magnetic-induction pickups were used to measure rotational motion of both the elevators and the rudder. Strain gages were attached to the aft-fuselage circular spar in order to indicate deflections in vertical bending, lateral bending, and torsion. An inclinometer and an accelerometer mounted near the model center of gravity measured the fuselage pitch angle and vertical translational motion, respectively. Another accelerometer was installed in the right nacelle to give an indication of nacelle vertical motion. All electrical leads were combined into a single umbilical cord which was brought out from the underside of the fuselage just below the center of gravity and was supported by the lower mounting cable.

Physical Properties

A summary of the model configurations and their physical properties is given in tables II and III and in figures 3 and 4. For simplicity and organization, the numerous configurations have been given coded designations. (See table II.) In this designation system, a letter indicates the design configuration or any major model component change from the design configuration. The first number designates the pitch spring used, and the last number indicates the amount of weight (in percent of design stabilizer weight) added at the tip of the design stabilizer. A small letter s is appended to some designations and means that the design stabilizer torsional stiffness has been increased by taping thin aluminum strips along the stabilizer span.

Stiffnesses.- Measured stiffness distributions for the major model components (stabilizer, fin, elevators, rudder, and aft fuselage) are presented in figure 4. In particular, distributions of bending and torsional stiffnesses for the fin with each of three interchangeable spars and for the stabilizer with each of two interchangeable spars are shown in figures 4(a) and 4(b), respectively. Note that the stiffnesses of the three fin spars are of comparable magnitude and that the stiffnesses of the two stabilizer spars are in close agreement. For some tests the stabilizer was stiffened by taping aluminum strips spanwise to the upper and lower surfaces near the leading edge. However, stiffnesses were not

measured for this condition. Stiffnesses of the stabilizer pitch springs and of the fin-stabilizer joints are given in table IV. Pitch spring 1 represents the design condition.

Masses.- The mass properties of the complete model, of the model components, and of the fin and stabilizer sections are given in table III. The masses of the three interchangeable fin spars were essentially the same, as were those of the two interchangeable stabilizer spars. For some tests, various amounts of concentrated mass were attached to the stabilizer spar on the elastic axis at the 96.5-percent-semispan station. (See table III(c).) Fuselage mass-distribution data are presented in figure 3. The two concentrated masses shown in figure 3 represent scaled masses of the airplane landing gear. Additional concentrated mass of up to 2 pounds was inserted in the fuselage nose as a counterbalance when the previously mentioned concentrated masses were attached to the stabilizer tips. The presence of this counterbalance mass did not appreciably affect the fuselage vibrational characteristics.

Natural frequencies and nodal patterns.- Measured symmetric- and antisymmetric-mode natural frequencies are presented in table V for the complete model mounted in the tunnel and for the cantilevered empennage. Nodal patterns shown in figures 5 to 13 are for the principal modes indicated in table V. Complete vibrational surveys were performed on the basic model configuration. (See table V and fig. 5(a).) Surveys following subsequent configuration changes generally covered only the modes which were considered to be significantly affected by the change.

Much of the nodal-pattern data presented in figures 5 to 13 is for the C-series configurations and was chosen for complete presentation for the following reasons: (1) a large amount of the vibrational data is available for these configurations, (2) configuration C1-0 did not differ appreciably from the design configuration A1-0, and (3) the effects on the natural frequencies and nodal patterns of changes in the mounting systems can be determined by direct comparison. As mentioned previously, stabilizer stiffnesses were not measured for the condition with added stiffening strips. However, the frequencies and nodal patterns for these configurations were examined. (See table V.)

A positive identification of the stabilizer natural pitch-mode frequency for the different pitch springs was not obtained during the investigation because of coupling effects between several important modes. Hence, following the tests a vibration study was conducted to determine the pitch frequencies for the various pitch springs by using configuration E cantilevered at fuselage station 158.8. The results are given in table V. However, the pitch-spring stiffnesses given in table IV were calculated from measured uncoupled pitch-spring frequencies. The natural-mode frequencies for pitch springs 1, 2, and 3 are generally consistent. However, the frequency for spring 4, which was considered to be essentially rigid, does not differ appreciably from that for design spring 1. This surprisingly low frequency of pitch spring 4 is attributed to flexibility in the pitch-spring support structure.

APPARATUS AND TESTS

Tunnel

This investigation was conducted in the Langley transonic dynamics tunnel which has a 16-foot-square test section (with cropped corners) and is a return-flow, variable-pressure, slotted-throat wind tunnel (ref. 10). It is capable of operation at stagnation pressures from near vacuum to slightly above atmospheric and at Mach numbers from 0 to 1.2. Mach number and dynamic pressure can be varied independently with either air or Freon-12 used as a test medium. The tunnel is equipped with a quick-opening bypass valve (ref. 10) which can be opened when flutter occurs in order to rapidly reduce the dynamic pressure in the test section.

Mount System

The model was supported in the tunnel by cables which were attached to the upper and lower end plates of the mounting cage previously described. (See fig. 1(d).) Two cables extended laterally forward from each end plate and were rigidly fastened to the sides of the tunnel. Two cables (one from each end plate) extended aft in a vertical plane, passed through the upper and lower center slots of the tunnel, and were spring-mounted outside the test section. This spring mount allowed freedom of the model in vertical translation, while flexure of the four vertical wires of the mounting cage permitted freedom in roll, pitch, and yaw as well as in lateral and longitudinal translation. Two auxiliary cables extended laterally forward from the model to reduce the drag loads on the mounting cage and to alleviate a Dutch roll tendency of the model. Initially, these auxiliary cables were attached to the under side of the wing beam at points near the wing-panel semispan (laterally, approximately opposite the model center of gravity). The cables extended through the tunnel sidewalls and were spring-mounted outside the test section. Subsequently, to improve the clarity of some nodal patterns on the tail and aft fuselage, these cables were replaced by a single continuous drag cable attached to the forward fuselage approximately midway between the nose and the center of gravity. This location was close to nodal points for several of the most important fuselage modes. The cable passed through the tunnel sidewalls and was supported by pulleys external to the test section. Outside the test section a sliding-friction yaw damper was installed on the cable but was found not to be required to maintain adequate lateral stability of the model.

Tests

Equipment.- During the tests, strain-gage and accelerometer signals from the model were continuously recorded on direct readout recorders and on magnetic tape. Visual records of model behavior were provided by high-speed motion pictures taken from the sides and rear. Tunnel conditions, such as tunnel stagnation and static pressures and stagnation temperature, were automatically digitized and printed by an IBM typewriter. For tests in Freon-12, the Freon purity was determined with a purity meter which sensed the variation of magnetic susceptibility of the oxygen

content of the testing medium. Freon-12 purity varied during the tests between 92 and 98 percent by volume (or 98.0 to 99.6 percent by weight).

Procedure.- Prior to testing, the model angle of attack and the stabilizer incidence angle were nominally set at 0°. Occasionally during the tests, it was necessary to remotely adjust the stabilizer incidence angle in order to relieve excessive static loads on the stabilizer.

Initially, a dynamic-pressure limit of 144 pounds per square foot was imposed on all tunnel tests on the basis of the model scaling parameters. However, this dynamic-pressure limit was exceeded frequently during the last part of the test program in attempts to define an antisymmetric flutter boundary. All tests in Freon-12 were limited to $M \leq 0.90$ which was approximately the design limit for the airplane. Tests in air were restricted to $M < 0.62$ because the model in air did not scale to the airplane at the higher Mach numbers. Investigations of control-surface instabilities were conducted only in air at very low dynamic pressures and Mach numbers because calculations and previous low-speed tests indicated that instabilities would be most likely to occur in this region.

The test procedure was essentially the same for tests in air and in Freon-12. This procedure is illustrated in figure 14 by a typical operating path (in Freon-12) described in terms of dynamic pressure as a function of Mach number. The operating sequence shown was employed in order to cover the desired ranges of dynamic pressure and Mach number in minimum running time. During some of the early tests, the model was occasionally excited both laterally and vertically at frequencies up to 20 cps by the shakers built into the fuselage nose. This practice was discontinued because at the higher dynamic pressures the model response to tunnel turbulence became greater than the response to shaker excitation. Tunnel conditions were recorded and high-speed motion pictures were taken whenever flutter occurred or at desired intervals. When flutter was observed, the tunnel bypass valve was opened and the tunnel fan speed was decreased in order to reduce rapidly the dynamic pressure in the test section. With one exception this technique prevented serious damage to the model.

PRESENTATION OF RESULTS

The experimental results of the present investigation are compiled in table VI. These data are shown in figures 15 to 21 in order to illustrate some flutter trends.

Figure 15 indicates the Reynolds number and Mach number ranges covered in the present tests. Flutter data obtained in air and in Freon-12 for configurations with control surfaces locked are presented in figures 16 and 17, respectively. Symmetric flutter data measured in air and in Freon-12 for two closely similar configurations have been adjusted to constant density in figure 18. Flutter data measured in air with a simulated free rudder, with simulated free elevators, and with simulated design symmetric-rotation stiffness of the elevators are shown in figures 19, 20, and 21, respectively.

DISCUSSION OF RESULTS

Control Surfaces Locked

The subcritical behavior of the model consistently involved both symmetric and antisymmetric motion. At low dynamic pressures the dominant response was nearly always antisymmetric (primarily fin torsion), and this relatively low-frequency motion increased in intensity as the dynamic pressure increased. Antisymmetric flutter, however, occurred only twice.[1] In all other instances, symmetric higher frequency response (mostly fin fore-and-aft bending and stabilizer pitching and bending) appeared and began to build and to override the antisymmetric motion as the dynamic pressure increased. The antisymmetric motion then gradually subsided, and in most cases symmetric flutter was attained or closely approached.

The difficulty in obtaining antisymmetric-flutter data led to the testing of several configurations which were devised to lower the antisymmetric-flutter boundary, to raise the symmetric-flutter boundary, or both. Although these configurations did not represent scaled conditions on the airplane, the results obtained indicate flutter trends and may be useful for theoretical correlation. These configurations (see table II) were obtained from the design configuration by (1) adding weights to the stabilizer tips because calculations and previous low-speed experiments had indicated that increasing stabilizer roll and yaw inertias tended to lower the antisymmetric flutter boundary, (2) taping aluminum strips along the stabilizer upper and lower surfaces near the leading edge and stiffening the pitch spring in order to stiffen the stabilizer against symmetrical torsional, bending, and pitching motion, (3) reducing torsional stiffness of the fin spar, or (4) replacing the rudder with a balsa fairing in order to eliminate any possibility that rudder hinge binding (during fin deflection) could contribute additional stiffness to the fin. The configurations which did correspond to possible physical conditions on the airplane were the design configurations and the configurations having weakened pitch springs to represent partial failure of the stabilizer pitch actuator.

Previous T-tail flutter investigations (for example, ref. 2) have indicated that increasing the horizontal-tail angle of attack would also lower the antisymmetric flutter boundary. In the present investigation, however, tail angles of attack were restricted to about $+1^{\circ}$ or less because of the rapid buildup of static loads on the horizontal tail.

Tests in air.- Results of the tests in air are presented in figure 16 in terms of the variation of dynamic pressure with flow density ρ and with mass ratio μ. As previously explained, all air tests were limited to low Mach numbers ($M < 0.62$) in order to avoid significant compressibility effects because the model in air does not scale to the airplane at the higher Mach numbers.

Design configuration: The design and near-design configurations (A1-0, A1-4, and C1-0) did not flutter within the Mach number and dynamic pressure ranges

[1]Since antisymmetric flutter was encountered only twice (in Freon-12 only), the term "flutter" as used in this section is understood to mean symmetric flutter unless otherwise indicated.

covered (table VI and fig. 16). For present purposes, the near-design configurations A1-4 and C1-0 are considered to be adequately representative of the design condition A1-0 for the following reasons: First, on the basis of this study and previous low-speed experiments, the addition of 4 percent mass to the stabilizer tips (configuration A1-4) would be expected to have an insignificant effect on symmetrical and antisymmetrical flutter properties. Second, the natural frequencies and nodal patterns for configuration C1-0 did not differ appreciably from those for configuration A1-0, the intended design configuration (table II), although fin spar 2 was somewhat weaker than fin spar 1, particularly in torsion (fig. 4(a)), and the rudder balance weights were not included in configuration C1-0. Therefore, configuration C1-0 is considered to be a conservative representation of the design configuration with regard to antisymmetric properties and essentially identical to the design configuration with regard to symmetric properties.

Pitch spring stiffness: Some effects of reducing the pitch-spring stiffness from the design level are shown in figure 16 by comparison of the results for configurations A1-0 (or C1-0), A2-0, and A3-0. Flutter occurred only with the weakest pitch spring (11 percent of design stiffness). The flutter motion at 27 cps involved significant deflections in bending, pitch, and torsion. The oscillations diverged rapidly and resulted in appreciable damage to the stabilizer including permanent deformation of stabilizer spar 1 and loss of the bullet fairing.

Stabilizer tip weights: Some previous low-speed experiments and calculations (unpublished) have indicated that increasing the stabilizer yaw and roll inertias by adding weights to the stabilizer tips lowered the antisymmetric flutter boundaries. Figure 16 shows that the symmetric flutter boundaries are also lowered by the addition of masses to the stabilizer tips (configurations A1-38 and A1-48). Comparison of the no-flutter points for near-design configurations A1-0, A1-4, and C1-0 with the flutter boundary for configuration A1-38 shows a sizable reduction in flutter speed caused by this addition of mass. The inclusion of an additional 10 percent mass (configuration A1-48) caused little further reduction in the flutter boundary except at the higher densities. The flutter encountered with configurations A1-38 and A1-48 was a high-frequency (60 to 62 cps), limited-amplitude, nondestructive motion involving primarily pitch and torsion.

Stiffened stabilizer and pitch spring: In an effort to obtain antisymmetric flutter by raising the symmetric flutter boundary, tests were made with a nearly rigid pitch spring (configuration A4-48) and with the stabilizer stiffened by metal strips taped near the leading edge (configuration C4-48s). Figure 16 shows that both model modifications raised the symmetric flutter boundary relative to that for configuration A1-48 but not enough to reach the antisymmetric flutter boundary. For densities near sea level, stiffening the pitch spring alone (configuration A4-48) increased the flutter dynamic pressure by about 10 percent; whereas, stiffening both the stabilizer and the pitch spring (configuration C4-48s) increased flutter q by about 30 percent. The flutter mode for these configurations was essentially the same as that for configuration A1-48. Since the objective of these model modifications was to obtain antisymmetric flutter, many of the tests were terminated in order to avoid the risk of model damage when the continuously recorded model response indicated that symmetric flutter was imminent. Many of the no-flutter points thus attained (fig. 16) appeared to be

very close to symmetric flutter, and these points formed the basis for the estimated flutter boundary shown in figure 16.

Tests in Freon-12.- Results of the tests in Freon-12 are presented in figure 17 in terms of the variations of dynamic pressure q and mass ratio μ with Mach number. In evaluating these data, it should be noted that reference 10 has indicated that subsonic and transonic flutter characteristics obtained in Freon-12 may reasonably be interpreted directly as equivalent data in air at the same mass ratio and Mach number. This direct interpolation, however, would result in a slightly conservative estimate of the flutter boundary, particularly at the higher Mach numbers. For example, for the present model at $M = 0.90$ the flutter dynamic pressure in air is estimated to be as much as 6 percent higher than that in Freon-12.

Design configuration: As shown in figure 17, the near-design configuration C1-0 did not flutter within the range of this investigation.

Stabilizer tip weights: Comparison of the flutter boundary for configuration C1-48 with the no-flutter points for configuration C1-0 (fig. 17) shows that, as in the low Mach number tests in air, the addition of 48 percent tip weights lowered the flutter boundary significantly. For configuration C1-48, the flutter boundary and the no-flutter points indicate that a minimum flutter dynamic pressure occurred near Mach number 0.8. The flutter mode for this configuration was essentially the same as that observed at low Mach numbers in air for configurations that included tip weights.

The flutter data shown in figure 17 for configuration C1-48 involve not only the effects of Mach number but also the effects of appreciable variations in mass ratio μ. In order to illustrate the effects of Mach number alone, these data have been adjusted (fig. 18) to indicate a flutter boundary for a constant density ($\rho = 0.0013$ slug/cu ft). The adjustment was based on the variation of dynamic pressure with density obtained from the low-speed tests in air for a similar configuration (A1-48). This modification appears reasonable on the basis of the flutter calculations of references 10 and 11 which indicate that for a given configuration the shape of the q-μ curve (for a constant M) generally does not vary appreciably over the subsonic range. Reference 10 also indicates that at the lower subsonic Mach numbers little difference would be expected between flutter boundaries in air and in Freon-12 at the same mass ratio. Hence, the low Mach number results in air are included in figure 18 to provide a reference for evaluating the magnitude of the compressibility effects. Although the adjustments for density are large in some cases, the resulting modified data form a single smooth curve which indicates that a maximum reduction in flutter dynamic pressure of about 16 percent occurs at a Mach number of about 0.78. However, reference 10 indicates that, as the Mach number increases, a flutter boundary in Freon-12 becomes increasingly conservative relative to the corresponding boundary in air at the same μ. Hence, the flutter boundary in air would be expected to show a smaller compressibility effect than the boundary in Freon-12.

Stiffened stabilizer and pitch spring: A comparison of the flutter boundary for configuration C1-48 with the no-flutter points for configuration C4-48s (fig. 17) shows that stiffening the stabilizer and pitch spring as described previously results in large increases in the flutter dynamic pressure. The increase

is as much as 100 percent or more at Mach numbers near 0.80. In contrast, the low Mach number tests in air indicated a corresponding increase of only about 30 percent. For the tests in Freon-12, however, the differences in mass ratio for configurations C1-48 and C4-48s probably account for a small portion of the increase. Although the stiffness increases raised the symmetric flutter boundary appreciably, no antisymmetric flutter was encountered within the q range covered.

Weakened fin spar: In further attempts to obtain antisymmetric flutter, the design fin spar (spar 1) was weakened in torsion and subsequently designated as spar 3. This reduction in stiffness together with an increase in stabilizer and pitch-spring stiffnesses, the inclusion of 48 percent tip weight, and an increase in the dynamic-pressure limit (above the limit for configuration C4-48s) resulted in two antisymmetric flutter points for configuration D4-48s. (See table VI and fig. 17.) Note that no flutter occurred when less tip weight was installed (configurations D1-0s and D1-26s). The two antisymmetric flutter points for configuration D4-48s were obtained in sequence during a single tunnel run; however, further attempts to attain flutter during the same and subsequent runs were unsuccessful even though the vicinity of these two antisymmetric flutter points was thoroughly explored to higher dynamic pressures. (See no-flutter points in fig. 17.) The reason for this nonreproducibility is not known. However, several possibly pertinent factors may be mentioned.

As indicated previously, static load limits on the model precluded testing over the complete range of stabilizer angle of attack anticipated for the airplane, even though this angle is recognized as an important parameter in antisymmetric flutter. When antisymmetric flutter occurred, the stabilizer appeared to be carrying a relatively large upward static load, and upward loading of the stabilizer characteristically contributes to a lowering of the antisymmetric flutter boundary (ref. 2, for example). In subsequent tests, the stabilizer incidence angle was approximately the same as when antisymmetric flutter occurred. It is possible, however, that during these subsequent tests, either the steady or the unsteady aerodynamic loads on the tail may have been altered by changing patterns of flow separation caused, for example, by adverse pressure gradients in the vicinity of the fin-stabilizer juncture, by the presence of the 0.02-inch-thick stiffening strips near the stabilizer leading edge, or by local shock disturbances. Factors of this type may influence the variation of T-tail antisymmetric-flutter boundaries with excitation amplitude which has been encountered by other investigators. (See refs. 5 and 12, for example.) In the present tests, tunnel turbulence at the higher dynamic pressures provided appreciable excitation amplitude in relation to the antisymmetric flutter amplitude. The tunnel turbulence, however, was random in nature and the use of large-amplitude harmonic excitation may have induced sustained flutter oscillations more readily. Nevertheless, the previously mentioned apparent suppression of antisymmetric response by the buildup of symmetric motion is worthy of additional investigation.

It is also possible that structural conditions in the model may have contributed to the nonrepeatability of the antisymmetric flutter points. However, it is not considered likely that any structural changes caused by motion of the model would result in an effective increase in stiffness and hence raise the flutter speed. Vibration surveys following each test did not indicate any significant changes in modal frequencies. Nevertheless, for the final two tests

the rudder was replaced by a balsa fairing in order to eliminate the possibility that rudder hinge binding could effectively add to the stiffness of the fin. For these two configurations, E4-48s and E4-94s, symmetric flutter occurred as shown in figure 17. For configuration E4-48s, the flutter was of the high-frequency (62 cps) type previously observed with configuration C1-48. The occurrence of this symmetric flutter at dynamic pressures lower than the antisymmetric flutter for configuration D4-48s is attributed to the fact that the stabilizer stiffening strips were attached differently for these two configurations so that the effective stiffness of configuration E4-48s was lower than that for configuration D4-48s.

The use of 94 percent tip weights (configuration E4-94s) yielded symmetric flutter in a different mode and at a much lower frequency (9 cps) than had been encountered with the other configurations. (See table VI and fig. 17.) This low-frequency flutter involved considerably more stabilizer bending than the high-frequency flutter previously discussed and occurred at considerably higher dynamic pressure than that for configuration E4-48s.

Control Surface Freedoms

Rudder and elevator freedoms were investigated with model configurations B1-0 and C1-0 which, for the purposes of these tests, were considered equivalent to the design configuration. The tests were conducted in air at very low densities and dynamic pressures where calculations and previous low-speed investigations had indicated that instabilities would most likely occur. Freedom of each control surface (rudder or elevator) was investigated separately while the other control remained locked at zero deflection. At each of the test points (figs. 19 to 21) except the single elevator-flutter point (fig. 20), the complete model was excited by the built-in shakers, and the amplitude of the control-surface rotation was measured as an indication of the proximity to instability.

Rudder.- Configuration B1-0 without rudder balance weights was investigated in a condition which simulated loss of rudder-actuator stiffness on the airplane (fig. 19). On the model, the rudder was allowed to rotate freely on the support flexures (fig. 1(c)) and had a rotational frequency of 4 cps. No instability was encountered at the test conditions shown in figure 19, although the amplitude of rudder response (fig. 19(b)) reached a maximum at a dynamic pressure of about 15 lb/sq ft. The flutter-boundary contour (shape only) (fig. 19(a)) was estimated from the subcritical rudder-response data by showing the boundary closest to the test points with the largest response; the levels of flow density associated with the shaded area in fig. 19(a) were arbitrarily chosen. The present results qualitatively confirm that unstable regions are more likely to occur at the lower dynamic pressures, as was indicated by previous low-speed tests and calculations (results unpublished).

Elevator.- Two different conditions of the 100-percent mass-balanced elevators were investigated (figs. 20 and 21). The first condition simulated loss of elevator-actuator stiffness on the airplane; the elevators of model configuration B1-0 were allowed to rotate freely on the support flexures and had a symmetric rotational frequency of about 10 cps. The second condition simulated the design symmetric rotation stiffness of the elevators (rotational frequency of 26 cps on the model) but had greater-than-design antisymmetric rotational stiffness. This

condition was considered to be an adequate representation of the airplane for present purposes because low-speed tests and calculations had indicated that any elevator instability would probably occur in a symmetric mode. For both conditions the elevator hinge shafts on the model were linked together by a universal joint.

The results for the elevator-free condition are shown in figure 20. One condition of self-excited symmetric flutter was encountered. The flutter motion at 21 cps appeared to consist of elevator rotation with no appreciable stabilizer motion. Flutter occurred at the beginning of the test and at that time the elevator-amplitude signals were not sufficiently amplified to yield accurate measurement of the flutter amplitude. However, the flutter amplitude was visually estimated to be about the same as the maximum subcritical-response amplitudes subsequently excited by the built-in shakers (fig. 20(b)). The flutter-boundary contour (shape only) estimated from the amplitude of the subcritical response (fig. 20) is in qualitative agreement with results of previous low-speed tests and calculations.

No instability occurred for the elevators with the design symmetric rotational stiffness (fig. 21). However, a flutter-boundary contour (shape only) has again been estimated from the amplitude of the subcritical response.

SUMMARY OF RESULTS

An experimental flutter investigation of a geometrically, dynamically, and elastically scaled model of the T-tail and aft fuselage of a currently projected multijet cargo airplane has been conducted in the Langley transonic dynamics tunnel at Mach numbers up to 0.90. The following results were obtained with control surfaces locked on configurations which represented scaled conditions on the airplane:

1. The design configuration did not flutter within the Mach number and dynamic pressure ranges covered.

2. A reduction in stabilizer-pitch-actuator stiffness to one-tenth of the design value resulted in a symmetric bending-pitch-torsion flutter of the stabilizer.

Results with control surfaces locked on configurations which did not represent scaled conditions on the airplane are as follows:

3. Addition to the stabilizer tips of concentrated weights equal to about one-half the stabilizer weight resulted in a high-frequency symmetric flutter involving primarily stabilizer pitch and torsion. This type of flutter was studied over a wide range of Mach number and density. With the concentrated weights increased to nearly the stabilizer weight, low-frequency symmetric pitch-bending-torsion flutter was encountered.

4. Two antisymmetric flutter points were obtained for a configuration having a weaker-than-design fin spar and incorporating stabilizer tip weights equal to

about one-half the stabilizer weight. In all other instances, symmetric motion appeared to override the antisymmetric response as dynamic pressure increased.

Results with control surface freedoms on configurations which represented scaled conditions on the airplane are as follows:

5. No instability occurred for a model condition which simulated loss of actuator stiffness for the zero mass-balanced rudder on the airplane.

6. No instability occurred for the 100-percent mass-balanced elevator with the design symmetric rotational stiffness. For the elevator-free condition, one self-excited symmetric flutter point was obtained.

Langley Research Center,
National Aeronautics and Space Administration,
Langley Station, Hampton, Va., October 22, 1963.

REFERENCES

1. Multhopp, Hans: The Case for T-Tails. Aero Digest, vol. 70, no. 5, May 1955, pp. 32-35.

2. Baldock, J. C. A.: The Determination of the Flutter Speed of a T-Tail Unit by Calculations, Model Tests and Flight Flutter Tests. Rep. 221, AGARD, North Atlantic Treaty Organization (Paris), Oct. 1958.

3. Goldman, R. L.: Flutter of T-Tails With Dihedral. ER 8205, The Martin Co., 1957.

4. Land, Norman S., and Fox, Annie G.: An Experimental Investigation of the Effects of Mach Number, Stabilizer Dihedral, and Fin Torsional Stiffness on the Transonic Flutter Characteristics of a Tee-Tail. NACA TN D-924, 1961. (Supersedes NACA RM L57A24.)

5. Pengelley, C. D., Wilson, L. E., Epperson, T. B., and Ransleben, G. E., Jr.: Flutter Characteristics of a T-Tail, WADC Tech. Rep. 52-162 (Contract No. AF 33(038)-18404), Wright Air Dev. Center, U.S. Air Force, Nov. 1954.

6. Stahle, C. V.: Transonic Effects on T-Tail Flutter. RM-24, The Martin Co., Feb. 1959.

7. Wasserman, Lee S.: Flutter Research of a T-Tail at Transonic Speeds. WADC Tech. Rep. 58-210, ASTIA Doc. No. AD 303424, U.S. Air Force, December 1958.

8. O'Hearne, C., and Numsen, G. N.: Vibration and Flutter Studies - Models YP6M-1 and P6M-2. Vol. I - Empennage Analyses. Eng. Rep. No. 9204-I (Contracts NOa(s)55-535 and NOa(s)57-161), The Martin Co., Nov. 1, 1957. (Revised June 10, 1958.)

9. Tomassoni, J. E., and Dietrick, D. L.: Vibration and Flutter Studies - Models YP6M-1 and P6M-2. Vol III - High Speed Flutter Models. Eng. Rep. No. 9204-III (Contracts NOa(s)55-535 and NOa(s)57-161), The Martin Co. (Revised Oct. 31, 1958.)

10. Yates, E. Carson, Jr., Land, Norman S., and Foughner, Jerome T., Jr.: Measured and Calculated Subsonic and Transonic Flutter Characteristics of a 45° Swept-back Wing Planform in Air and in Freon-12 in the Langley Transonic Dynamics Tunnel. NASA TN D-1616, 1963.

11. Yates, E. Carson, Jr.: Some Effects of Variations in Density and Aerodynamic Parameters on the Calculated Flutter Characteristics of Finite-Span Swept and Unswept Wings at Subsonic and Supersonic Speeds. NASA TM X-182, 1960.

12. Haviland, George P.: Wind-Tunnel Tests of a "Tee" Tail Flutter Model. Tech. Note WCLS-52-21, Wright Air Dev. Center, U.S. Air Force, Oct. 1952.

TABLE I.- GEOMETRIC PROPERTIES OF MODEL

Horizontal tail:	
Stabilizer with elevator:	
Aspect ratio	5.21
Sweepback angle of quarter-chord line, deg	25
Taper ratio	0.37
Airfoil section (streamwise)	NACA 64A010
Dihedral angle, deg	0
Area, sq ft	6.74
Mean aerodynamic chord, ft	1.217
Span, ft	5.92
Elastic-axis location, fraction of horizontal-tail chord (streamwise)	0.41
Length along elastic axis, ft	3.21
Elevator:	
Spanwise location, fraction of stabilizer semispan, at -	
Root	0.0625
Tip	1.00
Chordwise location, fraction of horizontal-tail chord (streamwise), at -	
Leading edge	0.724
Trailing edge	1.00
Hinge axis, fraction of horizontal-tail chord (streamwise)	0.750
Exposed area, fraction of horizontal-tail area	0.228
Horizontal-tail pivot axis, fraction of horizontal-tail chord at root (streamwise)	0.605
Vertical tail:	
Fin with rudder:	
Aspect ratio	1.24
Sweepback angle of quarter-chord line, deg	35
Taper ratio	0.61
Airfoil section (streamwise)	NACA 64_1A012
Area, sq ft	5.135
Mean aerodynamic chord, ft	2.073
Span, ft	2.53
Elastic-axis location, fraction of vertical-tail chord (streamwise)	0.40
Length along elastic axis, ft	2.74
Rudder:	
Spanwise location, fraction of fin span, at -	
Root	0
Tip	0.84
Chordwise location, fraction of vertical-tail chord (streamwise), at -	
Leading edge	0.716
Trailing edge	1.00
Hinge axis, fraction of vertical-tail chord (streamwise)	0.75
Exposed area, fraction of vertical-tail area	0.218

TABLE II.- SUMMARY OF MODEL CONFIGURATIONS

(a) Basic components

Basic configuration	Stabilizer spar	Fin spar	Rudder	Rudder mass balance, percent	Comments
A	1	1	Normal	100	Original components. Stabilizer damaged during tests.
B	2	1	Normal	0	Stabilizer spar 2 essentially same as spar 1. Slightly heavier bullet fairing used.
C	2	2	Normal	0	Fin spar 2 slightly weaker than spar 1.
D	2	3	Normal	0	Used fin spar weakest in torsion.
E	2	3	Replaced	---	Replaced rudder with balsa fairing.

(b) Tested configurations

Configuration	f_θ, cps	Horizontal tail				$\frac{m_v}{m_{v,o}}$	Comments
		$\frac{I_\theta}{I_{\theta,o}}$	$\frac{I_\psi}{I_{\psi,o}}$	$\frac{I_\phi}{I_{\phi,o}}$	$\frac{m_h}{m_{h,o}}$		
Configurations tested in air with control surfaces locked							
A1-0	99	1.000	1.000	1.000	1.000	1.000	Design configuration.
A2-0	57	1.000	1.000	1.000	1.000	1.000	Decreased pitch-spring stiffness.
A3-0	33	1.000	1.000	1.000	1.000	1.000	Decreased pitch-spring stiffness.
A1-4	94	1.107	1.192	1.185	1.042	1.000	Design configuration with light fairing for enclosing stabilizer tip weights.
A1-38	72	1.912	2.678	2.620	1.376	1.000	Added stabilizer tip weights to design configuration.
A1-48	67	2.178	3.170	3.098	1.483	1.000	Added stabilizer tip weights to design configuration.
A4-48	90	2.178	3.170	3.098	1.483	1.000	Increased pitch-spring stiffness. Efforts to obtain antisymmetric flutter.
C1-0	96	1.063	1.010	1.000	1.015	.955	Used slightly weaker fin spar (spar 2). Efforts to obtain antisymmetric flutter.
C4-48s	85	2.440	3.315	3.220	1.586	.955	Stiffened stabilizer and pitch spring. Efforts to obtain antisymmetric flutter.
Configurations tested in Freon-12 with control surfaces locked							
C1-0	96	1.063	1.010	1.000	1.015	0.955	Has weaker fin spar than design configuration.
C1-48	67	2.238	3.175	3.098	1.500	.955	Obtained symmetric flutter boundary over Mach number range.
C4-48s	85	2.440	3.315	3.220	1.586	.955	Stiffened stabilizer and pitch spring. Efforts to obtain antisymmetric flutter.
D4-48s	85	2.440	3.315	3.220	1.586	.955	Used weakest fin spar (spar 3). Efforts to obtain antisymmetric flutter.
D1-0s	88	1.265	1.150	1.131	1.100	.955	Efforts to obtain antisymmetric flutter.
D1-26s	72	1.902	2.325	2.268	1.363	.955	Efforts to obtain antisymmetric flutter.
E4-48s	85	2.440	3.315	3.220	1.586	.895	Replaced rudder. Efforts to obtain antisymmetric flutter.
E4-94s	71	3.543	5.330	5.170	2.034	.895	Added more tip weights. Efforts to obtain antisymmetric flutter.
Configurations tested in air with control surface freedoms							
B1-0	96	1.063	1.010	1.000	1.015	[a]1.015	Elevator locked. f_r = 4 cps.
B1-0	96	1.063	1.010	1.000	1.015	[a]1.015	Rudder locked. f_e = 10 cps.
C1-0	96	1.063	1.010	1.000	1.015	.955	Rudder locked. f_e = 26 cps. Very stiff antisymmetrically.

[a]Includes mass of solenoid attached to fin root to provide an impulse to rudder.

TABLE III.- MASS PROPERTIES OF MODEL CONFIGURATIONS

(a) Major model components

Total model (configuration A1-0):	
Mass, slugs	6.68
Center of gravity	FS 101.9
Fuselage mass, slugs	2.96
Wing and pylon-nacelle:	
Wing mass (full-span), slugs	1.878
Pylon-nacelle mass (both sides), slugs	1.467
Inertia in roll about fuselage center line, slug-ft^2	36.261
Empennage (configuration A1-0):	
Total empennage mass, slug	0.3787
Vertical tail mass, $m_{v,o}$, slug	0.1904
Horizontal tail:	
Mass, $m_{h,o}$, slug	0.1883
Center of gravity	FS 204.5
$I_{\theta,o}$, slug-ft^2	0.05665
$I_{\psi,o}$, slug-ft^2	0.3665
$I_{\phi,o}$, slug-ft^2	0.3559

TABLE III.- MASS PROPERTIES OF MODEL CONFIGURATIONS - Concluded

(b) Empennage components

Typical stabilizer without elevator				
Section (a)	Section limits, η_{ea}	Mass, slug	S_{ea}, slug-ft	I_{ea}, slug-ft^2
0	0 to 0.0586	0.0135	0.474×10^{-3}	0.692×10^{-3}
1	0.0586 to 0.2208	.0155	-.822	1.487
2	0.2208 to 0.3727	.0109	-.508	.654
3	0.3727 to 0.5234	.0092	-.343	.418
4	0.5234 to 0.6719	.0078	-.171	.296
5	0.6719 to 0.8255	.0063	-.120	.179
6	0.8255 to 1.0000	.0061	-.154	.150
Total	0 to 1.00	0.0693	-1.644×10^{-3}	3.876×10^{-3}

[a]Sections outlined on figure 1(b).

Typical fin without rudder				
Section (b)	Section limits, η_{ea}	Mass, slug	S_{ea}, slug-ft	I_{ea}, slug-ft^2
1	0 to 0.2648	0.0411	-1.15×10^{-3}	3.47×10^{-3}
2	0.2648 to 0.4728	.0323	-1.48	3.66
3	0.4728 to 0.6843	.0328	-2.13	3.47
4	0.6843 to 1.0000	.0604	-4.37	5.59
Total	0 to 1.00	0.1666	-9.13×10^{-3}	16.19×10^{-3}

[b]Sections outlined on figure 1(c).

Typical control surfaces				
Surface	Mass balance, percent	Mass, slug	S_{hl}, slug-ft	I_{hl}, slug-ft^2
Elevator	0	0.0107	0.645×10^{-3}	0.097×10^{-3}
Elevator	100	.0198	-.063	.156
Rudder	0	.0154	1.496	.367
Rudder	100	.0238	.128	.560

Bullet fairing				
Used with model configuration	Mass, slug	Center of gravity	I_ψ, slug-ft^2	I_θ, slug-ft^2
A	0.0101	FS 201.18	0.00504	0.00504
B, C, D, E	.0130	FS 198.85	.00914	.00868

(c) Stabilizer tip weights and stiffener

Tip weights:
- Spanwise location . . . . . BL 34.25
- Chordwise location . . . . . FS 212.32
- Mass (both panels):
  - 4 percent $m_{h,o}$, slug 0.00813
  - 26 percent $m_{h,o}$, slug 0.0497
  - 38 percent $m_{h,o}$, slug 0.0706
  - 48 percent $m_{h,o}$, slug 0.0914
  - 94 percent $m_{h,o}$, slug 0.1762

Stiffeners[c]:
- Mass (both panels), slug 0.0158
- Distance of center of gravity behind stabilizer leading edge, in. 1.0

[c]Stiffener extended along stabilizer from root to tip just behind leading edge.

TABLE IV.- STIFFNESSES OF STABILIZER PITCH SPRINGS

AND FIN-STABILIZER JOINTS

(a) Pitch-spring stiffness

Spring	Pitch stiffness, in-lb/radian
1	26.45×10^4
2	8.74
3	2.87
4	47.2

(b) Fin-stabilizer joint stiffness[a]

Fin spar	Yaw due to yawing moment, in-lb/radian	Yaw due to rolling moment, in-lb/radian	Roll due to yawing moment, in-lb/radian	Roll due to rolling moment, in-lb/radian
1	22.6×10^4	-28.7×10^4	-23.4×10^4	6.30×10^4
2	22.0	-30.0	-22.1	6.45
3	28.2	-39.6	-31.2	7.10

[a]Stiffnesses were measured between station on fin elastic axis at WL 59.50 and the point on underside of stabilizer spar at elastic axis where the bracket arm is attached. Sign convention of deflection and applied moments referenced to stabilizer chord plane:

Positive roll, right stabilizer tip downward;
positive yaw, right stabilizer tip rearward.

TABLE V.- MEASURED NATURAL FREQUENCIES OF MODELS

Vibration mode	Frequency, cps, of configuration for -																					
	Complete model											Empennage cantilevered at fin root					Empennage cantilevered at FS 158.8					
	A1-0 (a)	A1-0 (b)	B1-0 (b)	B1-3S (b)	C1-0 (b)	C3-0 (b)	C4-0 (b)	C4-48s (b)	C4-48s (c)	D1-0 (c)	D4-48s (c)	A1-0	C1-0	C2-0	C3-0	C4-0	E1-0s	E2-0s	E3-0s	E4-0s	D1-0s	D4-48
Symmetric modes																						
Model pitch		1.05								1.13												
Model vertical translation	1.20	1.40								1.60												
Model fore and aft translation		2.80								3.00												
Wing bending	9.9	9.5			*9.7					9.5												
Fuselage vertical bending	12.4	12.6	12.5		*12.8	12.2		*8.8		12.1												
Engine yaw					*15.0					14.7												
Fuselage vertical bending, stabilizer bending					*17.7												12.3				12.3	7.6
Stabilizer first bending	20.1	20.0	20.6	*13.8	*20.5	*20.1		*13.6		20.0		34.5	*34.0	*31.5	34.0	31.5	22.0				22.3	15.5
Fin fore and aft bending	24.4					*24.2				*24.0		16.4	*17.3	17.0	*17.3	17.8					25.9	33.0
	31.8							*28.8		*32.0							52.9				51.4	
								*42.2														
Stabilizer bending	61.0	61.8	60.8	*58.3	*63.0			*58.6		59.0				*47.5	*43.8		61.0					
Stabilizer pitch	71.0	70.0	69.9	*68.6	*70.1	*32.3	*71.1	*66.8		70.1		66.0	*68.5	*68.5	*56.5	*69.5	*70.5	*49.0	*44.0	*73.8	69.2	63.9
							*82.0	*71.6						*74.0	*68.8	74.5	77.5					
Stabilizer first torsion	83.0	81.0	81.7	*76.6	*84.4		*86.2	*81.8		85.0		76.3	*88.2	85.0	86.0	*86.0	88.5				87.2	74.3
															98.2							
					94			89.2					*97.4	103.5	102.0	99						
Stabilizer second torsion					120							121	120	119	120	118						
					137			136					135								143	
								182					140								178	
Antisymmetric modes																						
Model yaw		1.24																				
Model roll		1.26								1.25												
Model lateral translation		2.90								2.14												
Aft fuselage torsion	6.7	6.85	6.5	6.0	*7.4			*5.2	*4.9	*6.6	*4.9											
Stabilizer roll	10.7	10.2	11.2	*9.1	*9.1			*7.3	*6.7	*10.2	*6.4	9.3	*9.2				7.1				7.1	
Stabilizer yaw	13.9	13.9	12.6		*11.5			11.4	*9.6	*12.8	*9.6	13.3	*12.8	13.0	13.0	13.0	11.0				10.8	
Stabilizer yaw, fuselage lateral bending	15.8	15.8	15.8		*14.3			*15.0	*14.8	15.6	*14.8	20.4	*19.5				16.6				16.5	
											*16.0											
Fin bending	18.5	18.8	19.0		*19.3			*18.2		18.8												
Stabilizer bending, fin bending	25.0	26.7	26.0	*25.3	*26.4			*25.1		25.0	*25.0											
				*38.8						44.0												
	53.0	54.0	53.2	*45.0	*56.7			*45.3		55.0	*42.6	54.0	*54.2									
													*56.9				58.0				57.0	
	65.2	66.3	65.9		*65.1			*63.3		63.5			*63.5									
								*73.8														
					70.2			*77.2		75.0							77.0				73.0	
Stabilizer first torsion	80.0	82.0	82.9	*74.5	*82.9			*83.8		82.5		80	*90.8				81.8				78.0	
					102			*97.6														
					107			112													111	
					115			117														
Stabilizer second torsion					138							135	135									

[a] Model suspended by single vertical spring at upper plate of mount cage.

[b] Model mounted in tunnel with drag cables at wing midsemispan (cables 7 and 8 in fig. 1(d)). Used in tests 1 to 12, 24, and 25.

[c] Model mounted in tunnel with drag cable at midsection of forward fuselage (cable 9 in fig. 1(d)). Used in tests 13 to 23 and 26.

* Node lines for these modes are presented in figures 5 to 13.

TABLE VI.- COMPILATION OF TEST RESULTS

(a) Tests in air with control surfaces locked

Configuration	Run point	Model behavior (a)	M	q, lb/sq ft	ρ, slug/cu ft	V, ft/sec	T, °R	μ	f, cps	N_{Re}/ft
A1-0	1-1	NF	0.308	141.3	0.002278	352.0	544	12.8		2.07×10^6
A2-0	2-1	NF	.472	144.5	.000997	538.3	541	29.3		1.39
A3-0	3-1	SF	.442	135.4	.001063	504.3	543	27.5	27	1.38
A1-4	4-1	NF	.416	146.1	.001316	471.3	534	23.1		1.62
A1-38	5-1	SF	.385	97.8	.001019	438.3	539	39.4	62	1.16
	5-2	SF	.363	101.5	.001182	414.5	543	34.0	62	1.26
	5-3	SF	.348	111.5	.001408	397.9	544	28.5	62	1.44
	5-4	SF	.334	119.2	.001631	382.3	545	24.6	62	1.61
	5-5	SF	.318	130.5	.001963	364.7	547	20.4	62	1.84
	5-6	SF	.308	139.9	.002239	353.6	548	17.9	62	2.03
A1-48	6-1	SF	.382	94.0	.000991	435.5	541	43.8	60	1.12
	7-1	SF	.344	108.4	.001422	390.4	536	30.5	60	1.45
	8-1	SF	.292	127.1	.002271	334.6	546	19.1	60	1.95
A4-48	9-1	SF	.304	139.8	.002267	351.2	548	19.1	60	2.04
C1-0	10-1	NF	.413	147.6	.00132	472.0	544	22.5		1.61
C4-48s	11-1	[b]NF	.563	69.3	.000349	629.9	521	132.6		.59
	11-2	[b]NF	.619	82.2	.000343	692.0	520	134.9		.63
	11-3	[b]NF	.612	90.8	.000386	685.9	523	119.9		.70
	11-4	[b]NF	.592	91.4	.000413	665.6	526	112.0		.73
	11-5	[b]NF	.568	96.1	.000468	640.9	530	98.9		.79
	11-6	[b]NF	.533	99.0	.000545	603.0	533	84.9		.86
	11-7	[b]NF	.503	101.6	.000624	570.8	536	74.1		.93
	11-8	[b]NF	.473	104.8	.000724	538.2	539	63.9		1.01
	12-1	[b]NF	.449	111.6	.000901	497.7	511	51.3		1.21
	12-2	[b]NF	.434	117.8	.00102	480.8	511	45.4		1.33
	12-3	[b]NF	.402	114.4	.00115	446.5	513	40.2		1.39
	12-4	[b]NF	.404	129.2	.00128	448.7	513	36.1		1.55
	12-5	[b]NF	.387	131.1	.00142	430.3	515	32.6		1.64
	12-6	[b]NF	.374	135.7	.00157	416.2	516	29.5		1.75
	12-7	[b]NF	.365	144.3	.00174	406.9	517	26.6		1.90
	12-8	[b]NF	.353	151.6	.00195	393.9	518	23.7		2.06
	12-9	SF	.348	162.8	.00216	388.1	518	21.4	65	2.24
	13-1	[b]NF	.452	96.3	.000774	499.0	507	59.8		1.05
	13-2	[b]NF	.450	112.9	.000899	501.1	516	51.5		1.21
	13-3	[b]NF	.412	118.3	.001109	462.0	523	41.7		1.36
	13-4	[b]NF	.380	125.7	.001365	429.1	531	33.9		1.54
	13-5	[b]NF	.355	133.6	.001648	402.7	536	28.1		1.73
	13-6	[b]NF	.327	146.4	.002093	374.0	544	22.1		2.02

[a]Model behavior code:
NF No flutter
SF Symmetric flutter
AF Antisymmetric flutter

[b]No flutter, but very close to symmetric flutter boundary.

TABLE VI.- COMPILATION OF TEST RESULTS - Continued

(b) Tests in Freon-12 with control surfaces locked

Configuration	Run point	Model behavior (a)	M	q, lb/sq ft	ρ, slug/cu ft	V, ft/sec	T, °R	γ	R, $ft^2/sec^2/°R$	μ	f, cps	N_{Re}/ft
C1-0	14-1	NF	0.897	138.2	0.001324	456.1	521	1.140	433	22.4		2.24×10^6
	14-2	NF	.867	144.0	.001459	443.2	530	1.138	432	20.3		2.38
	14-3	NF	.782	147.0	.001826	400.2	537	1.137	428	16.2		2.68
	14-4	NF	.697	149.2	.002330	356.7	542	1.135	425	12.7		3.05
	14-5	NF	.633	152.3	.002903	322.6	543	1.135	422	10.2		3.45
C1-48	15-1	NF	.903	67.8	.000663	452.0	516	1.137	424	66.1		1.14
	15-2	NF	.903	74.5	.000724	453.3	517	1.138	426	60.5		1.24
	15-3	NF	.904	82.7	.000796	455.2	523	1.136	424	55.0		1.37
	15-4	NF	.892	86.6	.000846	551.6	530	1.135	423	51.8		1.43
	15-5	SF	.825	88.5	.001041	411.7	513	1.138	425	42.1	60	1.63
	15-6	SF	.737	89.1	.001310	368.2	518	1.137	422	33.4	60	1.84
	15-7	SF	.799	76.4	.000936	403.4	527	1.136	423	46.8	60	1.42
	15-8	SF	.815	76.3	.000886	414.3	535	1.135	423	49.5	60	1.36
	15-9	SF	.664	108.6	.001935	334.1	534	1.134	417	22.6	60	2.44
	15-10	SF	.598	125.9	.002795	299.0	532	1.134	415	15.7	60	3.18
C4-48s	16-1	NF	.906	103.1	.000969	460.6	521	1.139	433	47.7		1.66
	16-2	NF	.901	135.3	.001281	458.6	532	1.137	427	36.1		2.18
	16-3	NF	.871	146.9	.001471	445.8	539	1.135	426	31.5		2.41
	16-4	NF	.792	151.5	.001821	406.8	548	1.134	423	25.4		2.71
	16-5	NF	.702	154.1	.002353	360.7	554	1.133	421	19.7		3.10
	16-6	NF	.669	159.9	.002685	343.9	558	1.132	420	17.2		3.37
D4-48s	17-1	NF	.917	103.0	.001011	451.0	508	1.137	417	45.8		1.78
	17-2	NF	.896	150.5	.001483	449.5	524	1.136	421	31.2		2.52
	17-3	NF	.827	163.0	.001859	417.7	534	1.135	420	24.9		2.91
	17-4	NF	.769	173.8	.002256	391.3	544	1.133	419	20.5		3.27
	18-1	[b]AF	.779	177.4	.002269	394.1	541	1.133	417	20.4	6.22	3.34
	18-2	[b]AF	.745	179.7	.002462	380.8	552	1.132	418	18.8	6.33	3.45
	18-3	NF	.803	168.2	.001996	409.4	548	1.133	419	23.2		3.02
	18-4	NF	.794	178.5	.002154	405.8	551	1.132	419	21.5		3.22
	18-5	NF	.724	174.5	.002509	371.6	558	1.131	418	18.5		3.40
	18-6	NF	.768	201.4	.002549	396.2	563	1.131	418	18.1		3.67
	19-1	NF	.772	202.4	.002635	390.5	530	1.138	425	17.6		3.83
	19-2	NF	.780	188.5	.002349	399.3	543	1.135	425	19.7		3.44
D1-0s	20-1	NF	.825	156.2	.001820	413.3	521	1.138	423	17.6		2.85
	20-2	NF	.758	173.7	.002363	382.2	532	1.136	420	13.6		3.39
	20-3	NF	.798	188.1	.002310	402.2	533.1	1.135	420	13.9		3.49
	20-4	NF	.776	210.7	.002701	393.6	541	1.134	419	11.9		3.96
	20-5	NF	.698	201.0	.003127	357.1	553	1.133	418	10.3		4.10
D1-26s	21-1	NF	.887	114.4	.001168	442.0	517	1.137	420	33.0		1.97
	21-2	NF	.758	187.1	.002533	383.0	543	1.133	415	15.2		3.63
E4-48s	22-1	NF	.740	137.9	.002010	369.3	527	1.135	416	23.0		2.83
	22-2	SF	.689	146.3	.002457	344.0	530	1.134	415	18.8	62.5	3.22
	22-3	SF	.659	168.0	.003048	330.7	538	1.133	414	15.2	62.5	3.81
E4-94s	23-1	NF	.794	156.2	.001926	401.6	530	1.137	424	30.7		2.89
	23-2	SF	.806	192.2	.002273	409.9	541	1.134	421	26.0	9.33	3.45
	23-3	NF	.731	205.9	.002943	372.6	548	1.133	419	20.1		4.05

[a]See footnote a, p. 25.

[b]Antisymmetric flutter occurred with a stabilizer incidence angle of $-\frac{1}{2}^\circ$ (nose down) and a stabilizer angle of attack of approximately $1\frac{1}{2}^\circ$ (nose up).

TABLE VI.- COMPILATION OF TEST RESULTS - Concluded

(c) Tests in air with control surface freedoms

Configuration	Run point	Model behavior (a)	M	q, lb/sq ft	ρ, slug/cu ft	V, ft/sec	T, °R	μ	f, cps	$\frac{A_{max}}{A}$	N_{Re}/ft
B1-0	24-1	NF	0.183	9.0	0.000454	198.7	491	65.3		1.05	0.25 × 10^6
(rudder	24-2	NF	.229	14.0	.000453	248.9	492	65.4		1.00	.31
free,	24-3	NF	.267	19.0	.000452	290.2	492	65.6		1.00	.37
f_r = 4 cps)	24-4	NF	.298	23.8	.000452	324.1	492	65.6		1.15	.41
	24-5	NF	.327	28.6	.000451	356.0	493	65.7		1.28	.45
	24-6	NF	.377	38.0	.000448	411.4	496	66.2		1.79	.51
	24-7	NF	.420	47.1	.000446	459.6	498	66.5		1.79	.57
	24-8	NF	.493	64.9	.000441	542.5	504	67.2		1.92	.65
B1-0	25-1	SF	.200	9.1	.000363	223.5	520	81.7	21	[b]1.50	.22
(elevator	25-2	NF	.130	3.9	.000365	146.2	527	81.2			.14
free,	25-3	NF	.162	6.1	.000367	182.1	526	80.8		7.13	.18
f_e = 10 cps)	25-4	NF	.184	8.0	.000378	206.4	524	78.4		2.46	.21
	25-5	NF	.194	9.0	.000379	217.5	523	78.2		2.37	.22
	25-6	NF	.203	9.9	.000383	227.4	522	77.4		1.94	.23
	25-7	NF	.213	10.9	.000384	238.5	521	77.2		1.60	.24
	25-8	NF	.222	11.9	.000385	248.5	521	77.0		1.16	.26
	25-9	NF	.230	12.8	.000386	257.4	521	76.8		1.33	.26
	25-10	NF	.247	14.8	.000388	276.1	520	76.4		1.00	.29
	25-11	NF	.256	16.0	.000391	285.9	519	75.8		1.33	.30
	25-12	NF	.262	16.8	.000392	292.5	519	75.6		1.49	.31
	25-13	NF	.278	19.0	.000394	310.1	518	75.2		1.06	.33
	25-14	NF	.290	20.7	.000396	323.2	517	74.9		2.00	.34
	25-15	NF	.308	23.3	.000397	343.0	516	74.7		2.91	.37
	25-16	NF	.339	28.3	.000398	376.9	514	74.5		3.77	.40
	25-17	NF	.368	33.2	.000398	408.4	513	74.5		4.27	.44
	25-18	NF	.390	37.5	.000401	432.6	512	73.9		3.99	.47
	25-19	NF	.438	46.9	.000399	484.4	509	74.3		4.62	.52
	25-20	NF	.193	9.8	.000420	216.5	524	70.6		2.28	.24
C1-0	26-1	NF	.171	5.2	.000289	188.9	509	102.6		2.50	.15
(elevator	26-2	NF	.240	10.1	.000286	265.4	509	103.6		2.84	.21
with	26-3	NF	.293	14.89	.000283	324.1	509	104.7		6.25	.25
simulated	26-4	NF	.338	19.63	.000280	374.3	510	105.9		6.25	.28
symmetric	26-5	NF	.378	24.34	.000277	419.0	511	107.0		7.80	.31
design	26-6	NF	.416	29.23	.000276	460.6	510	107.4		11.70	.34
stiffness,	26-7	NF	.448	33.66	.000272	497.1	512	109.0		11.70	.37
f_e = 26 cps)	26-8	NF	.477	38.05	.000270	531.4	516	109.8		12.50	.39
	26-9	NF	.507	42.66	.000267	565.3	517	111.0		11.35	.40
	26-10	NF	.239	10.34	.000280	271.6	539	105.9		1.98	.20
	26-11	NF	.175	5.58	.000283	198.7	537	104.7		1.37	.15
	26-12	NF	.140	3.58	.000286	158.3	532	103.6		1.00	.12

[a] See footnote a, p. 25.

[b] Estimated.

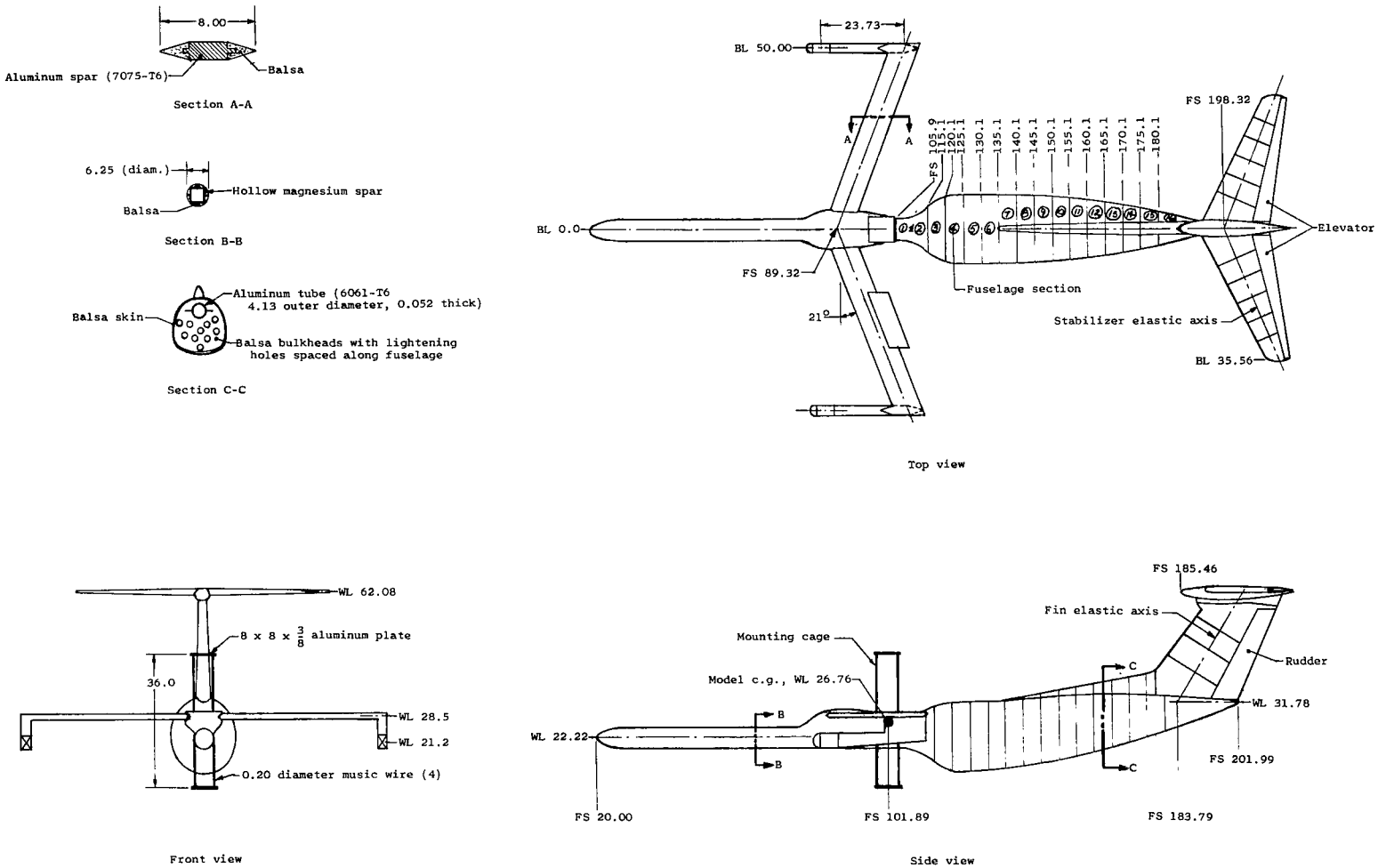

(a) Complete model.

Figure 1.- Sketches of model. All dimensions are in inches except as noted otherwise.

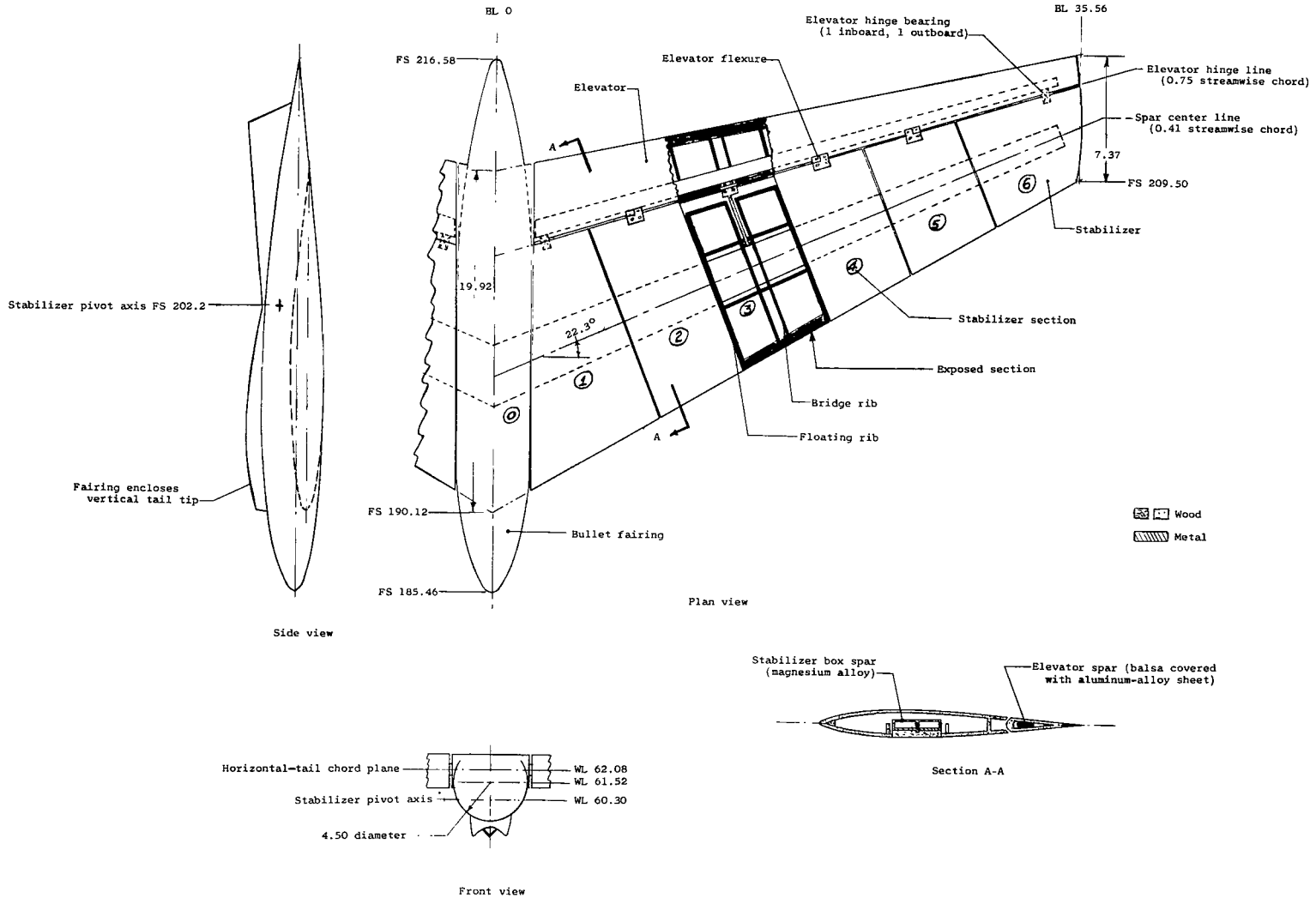

(b) Horizontal tail.

Figure 1.- Continued.

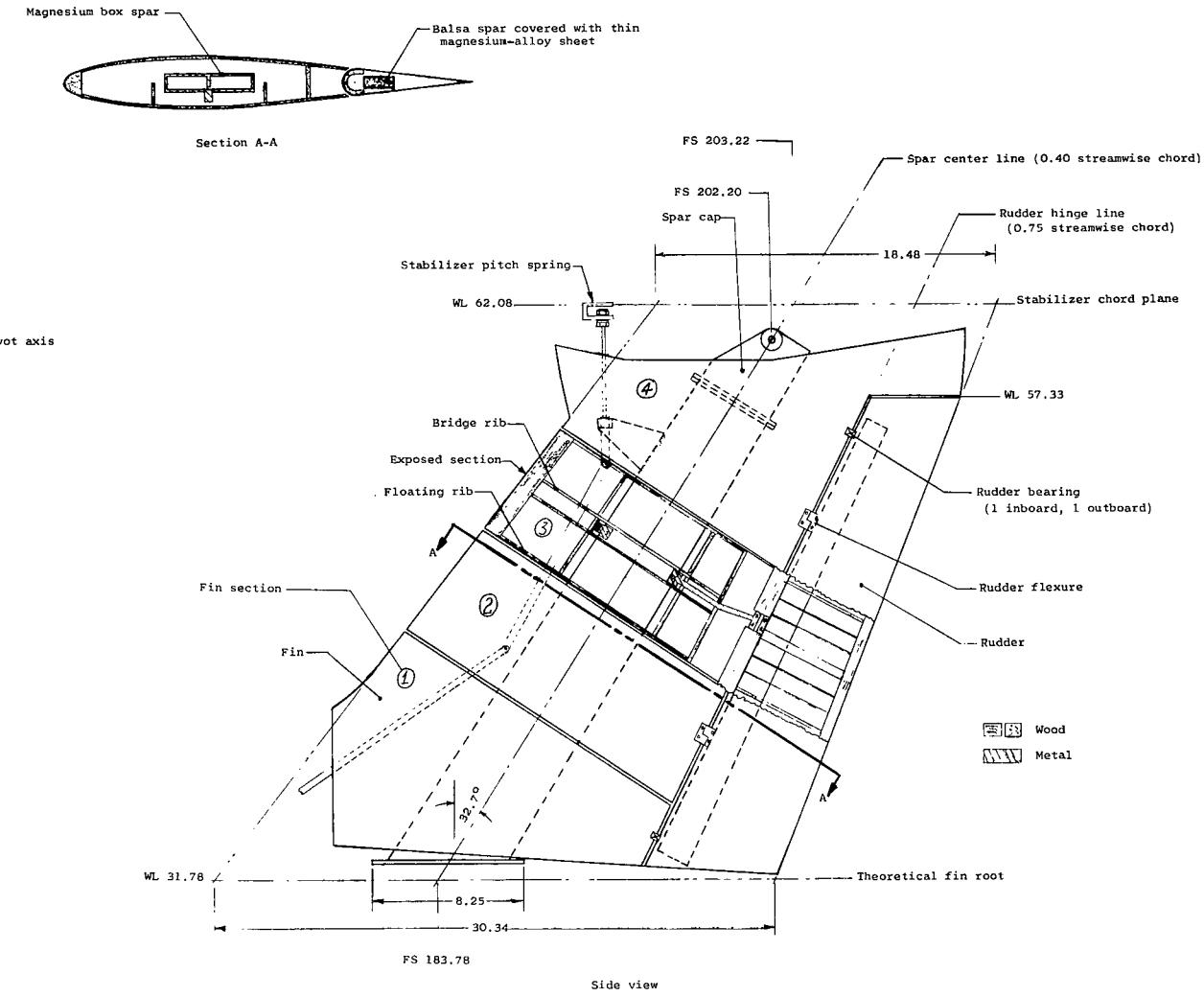

(c) Vertical tail.

Figure 1.- Continued.

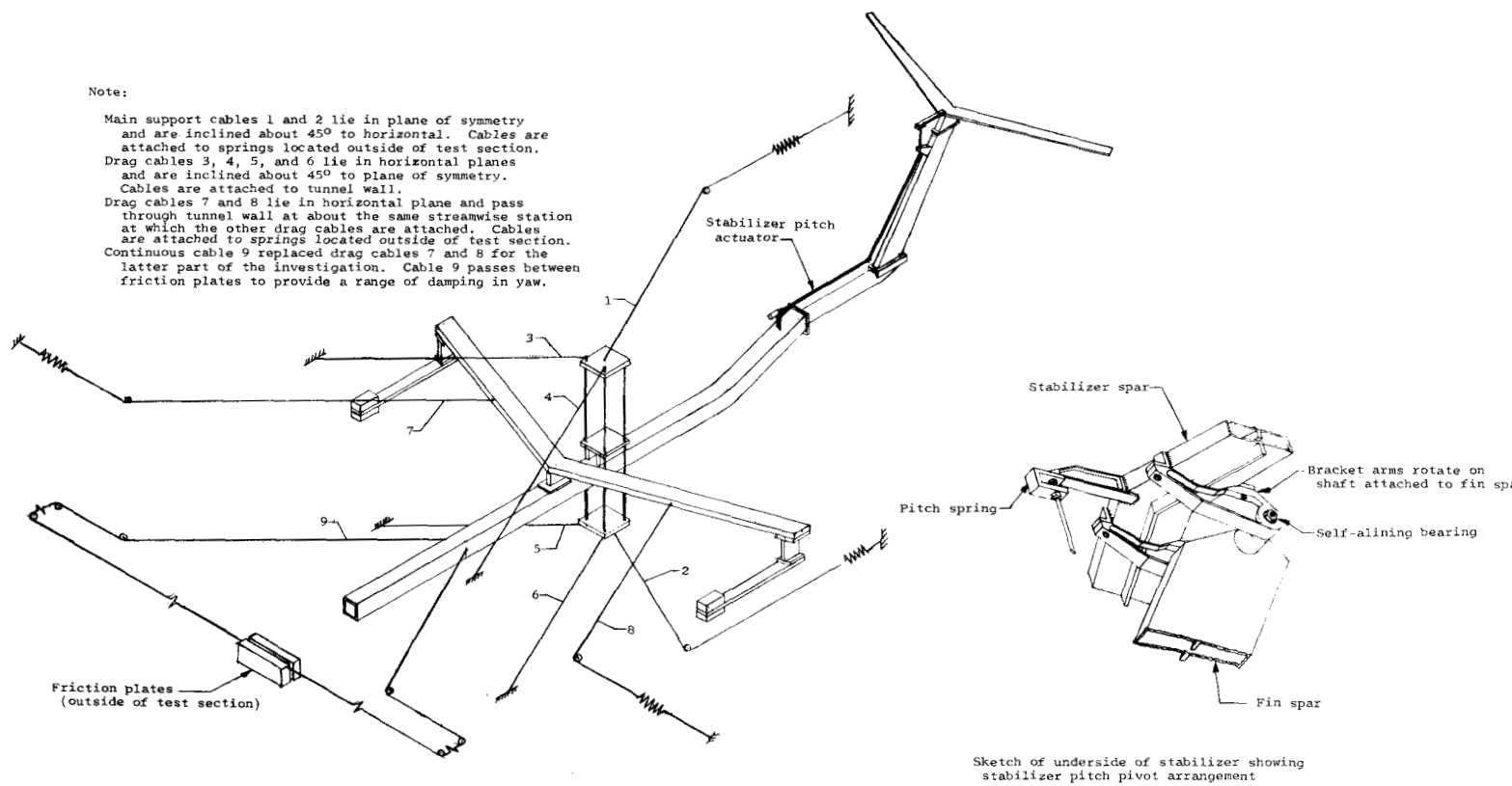

Sketch of underside of stabilizer showing stabilizer pitch pivot arrangement

(d) Sketch showing main structural members of model and mount system.

Figure 1.- Concluded.

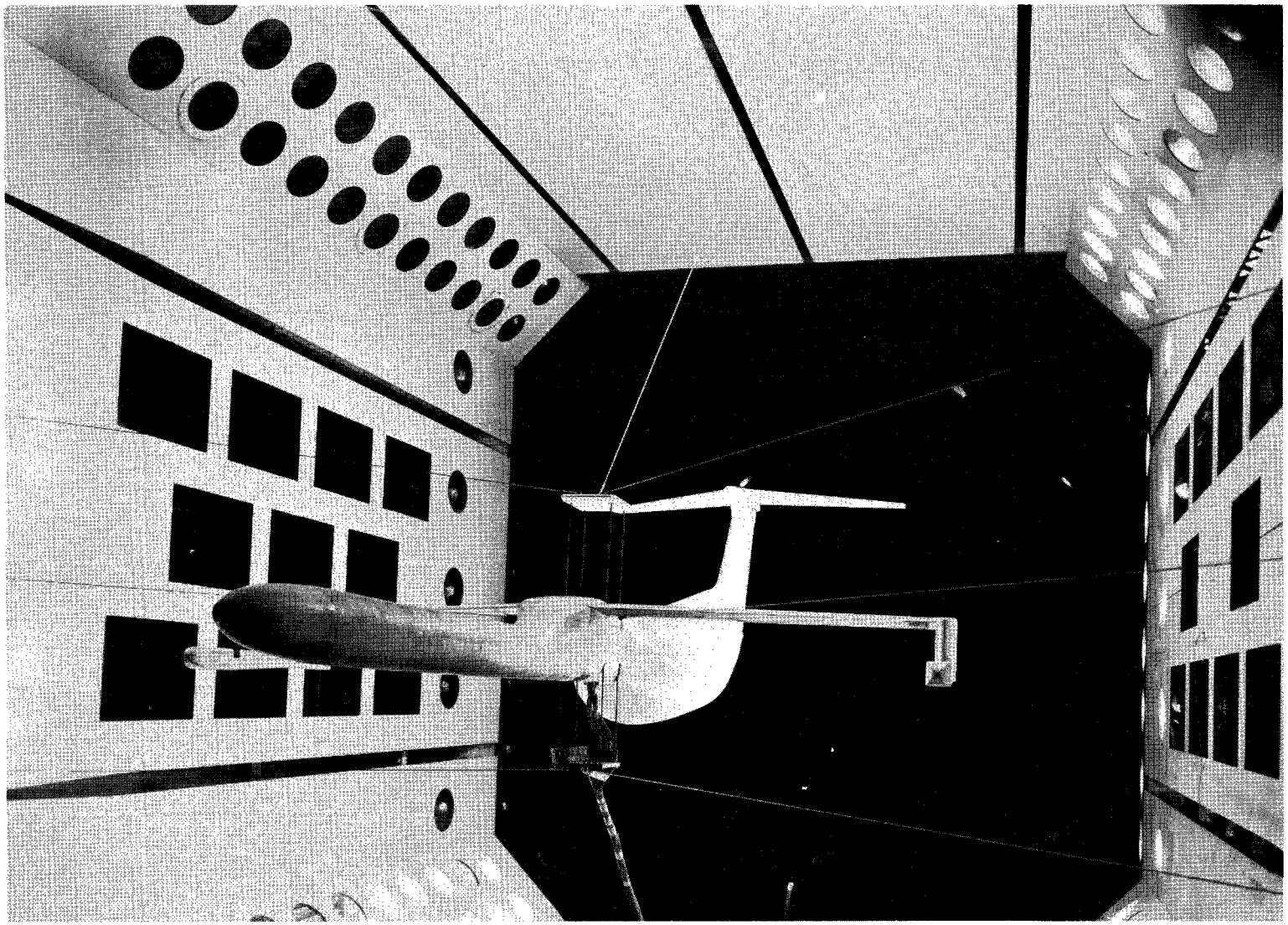

(a) Model suspended in tunnel. L-61-8745

Figure 2.- Model used in the investigation.

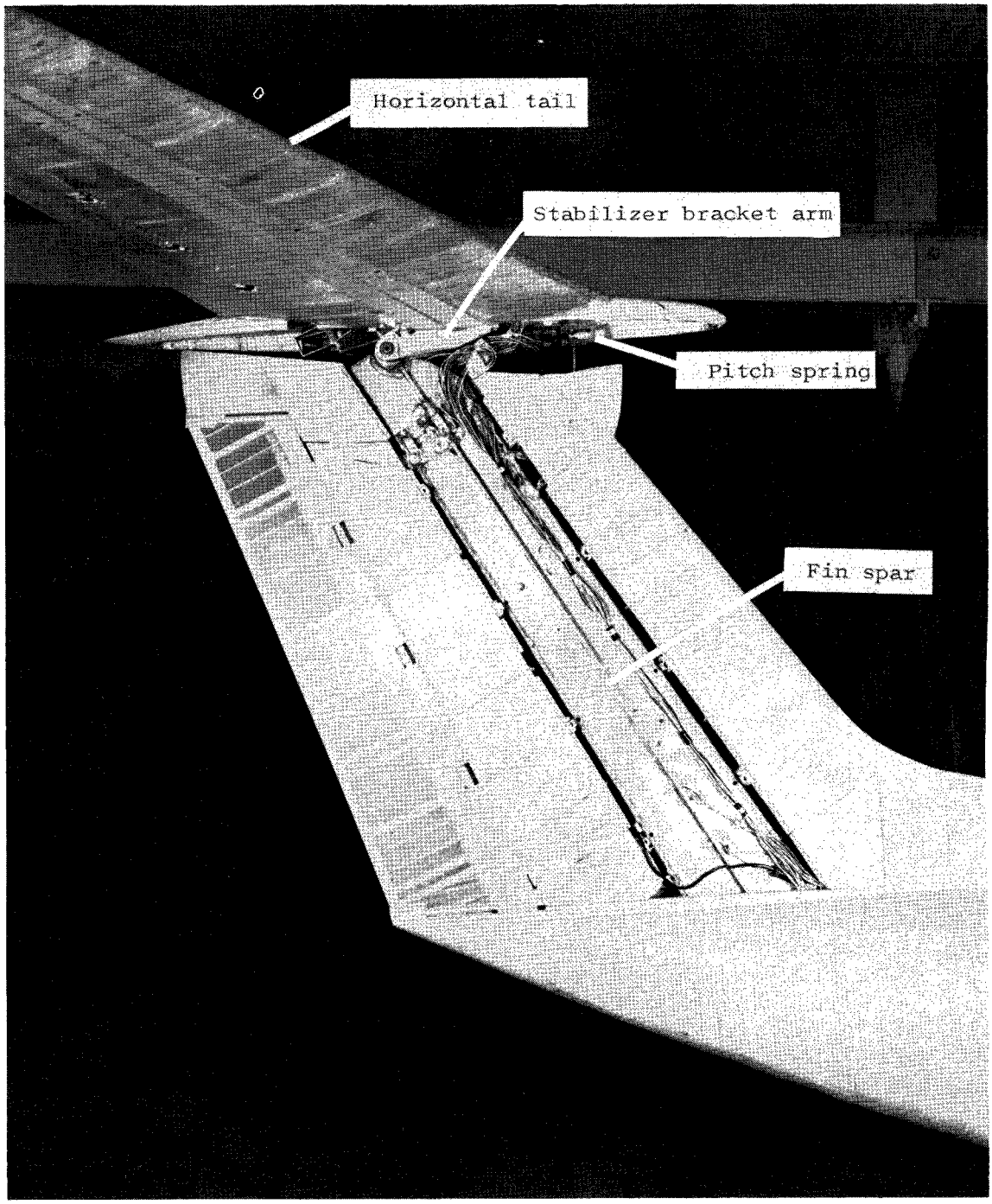

(b) Vertical tail with fin-spar cover and lower half of bullet fairing removed. L-61-8491.1
Rudder is locked by tape at tip and root.

Figure 2.- Concluded.

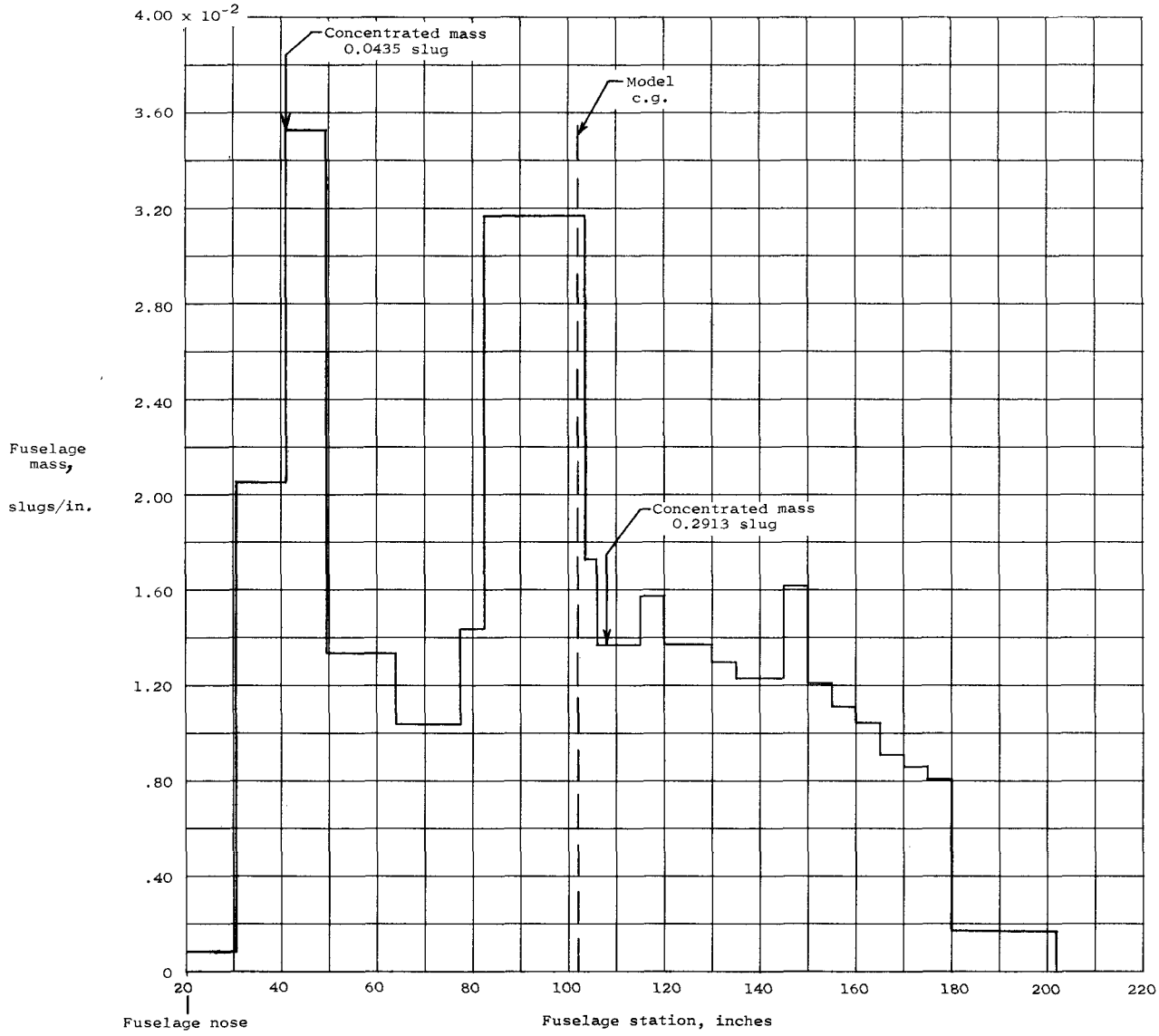

Figure 3.- Fuselage mass distribution

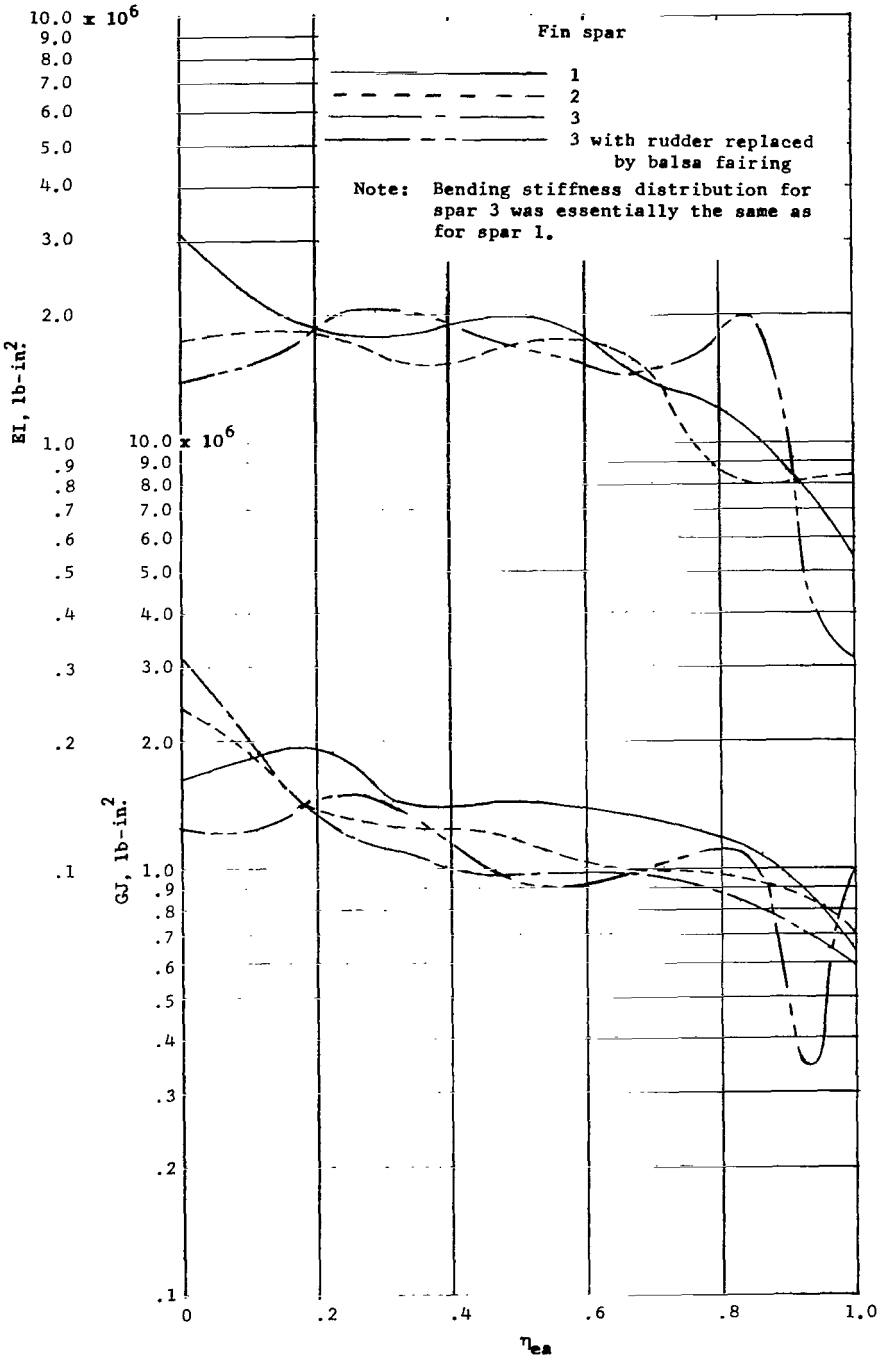

(a) Fin spars.

Figure 4.- Measured distribution of bending and torsional stiffnesses of various model structural components.

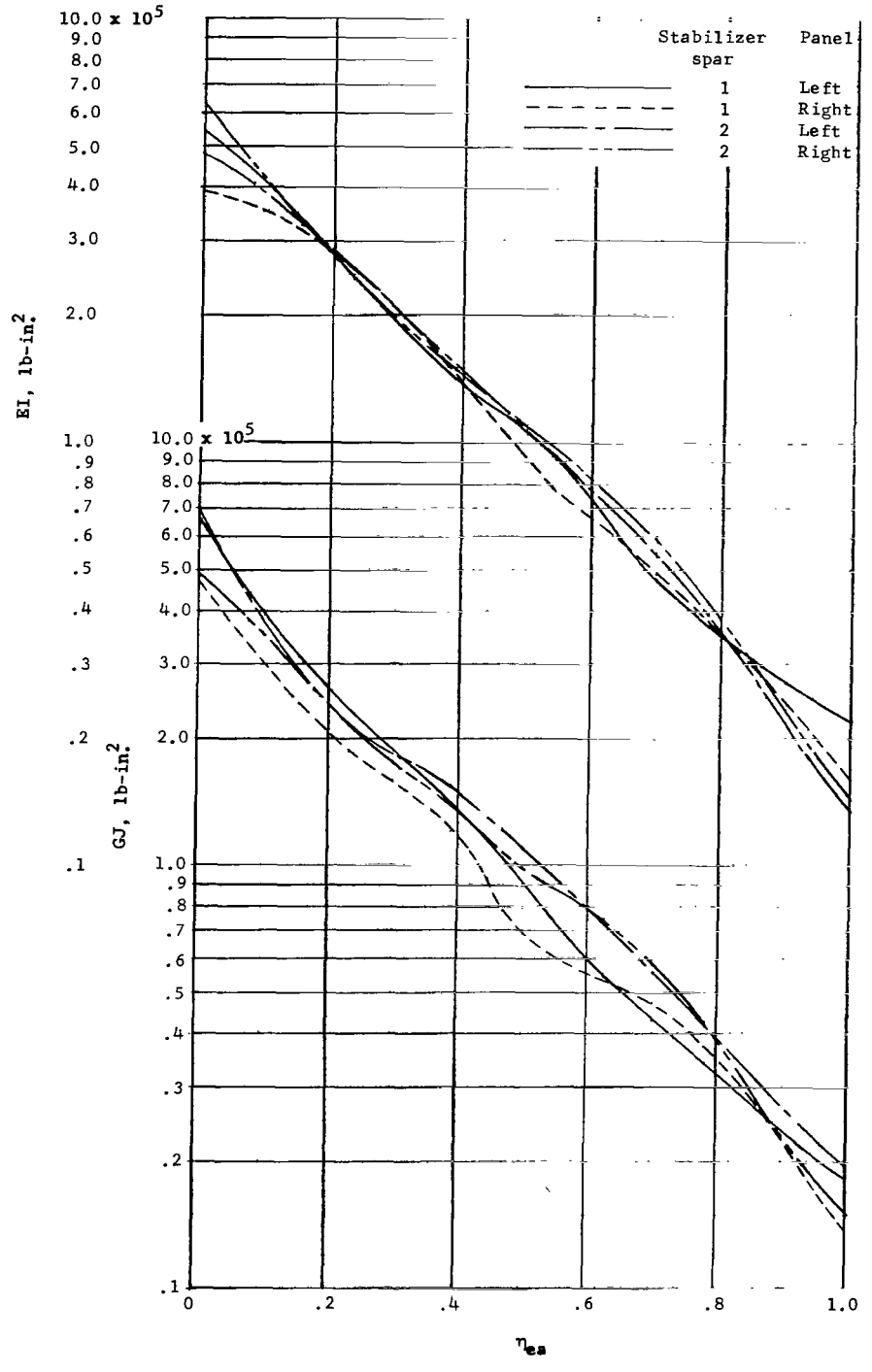

(b) Stabilizer spars.

Figure 4.- Continued.

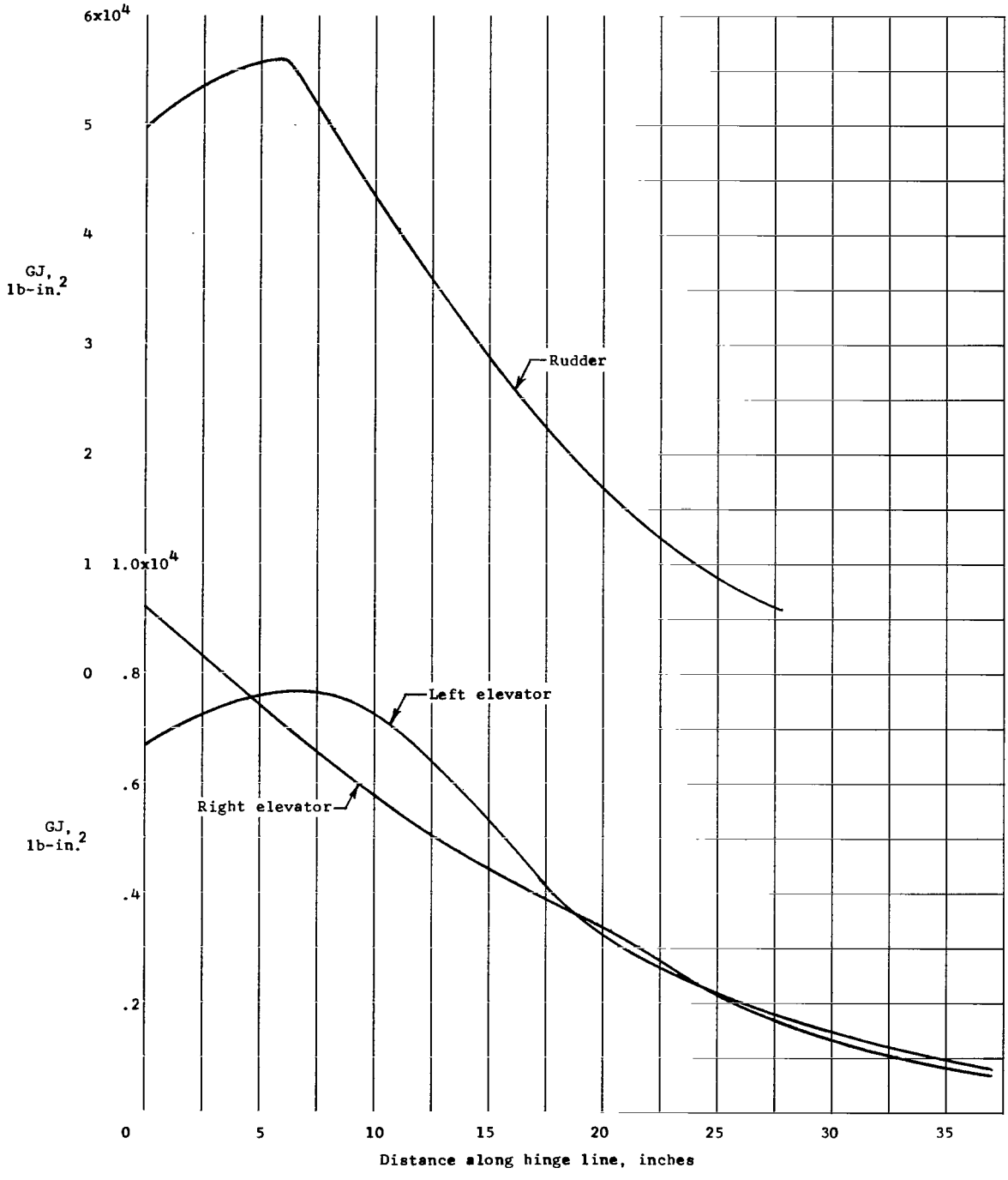

(c) Rudder and elevator.

Figure 4.- Continued.

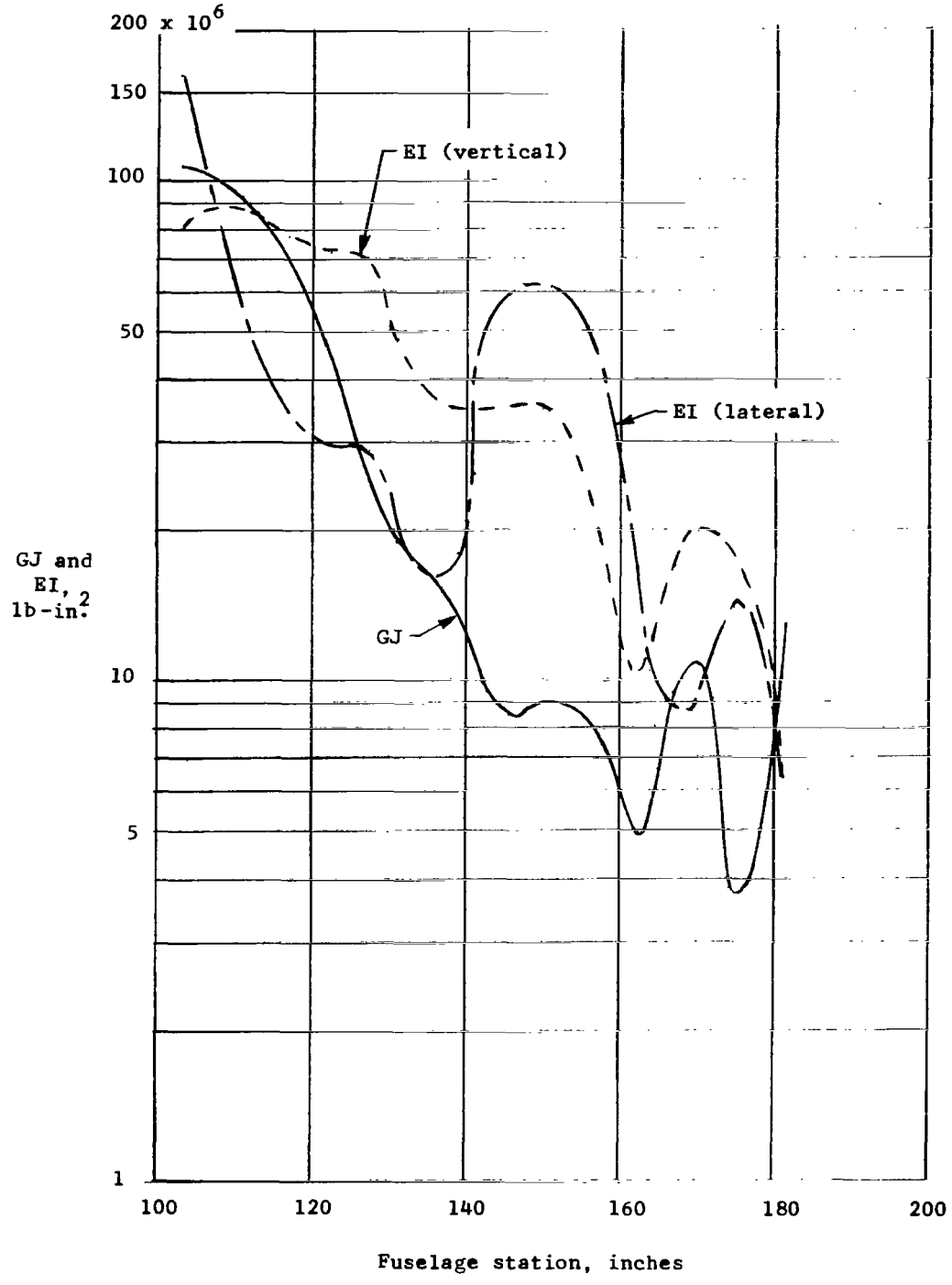

(d) Aft fuselage spar.

Figure 4.- Concluded.

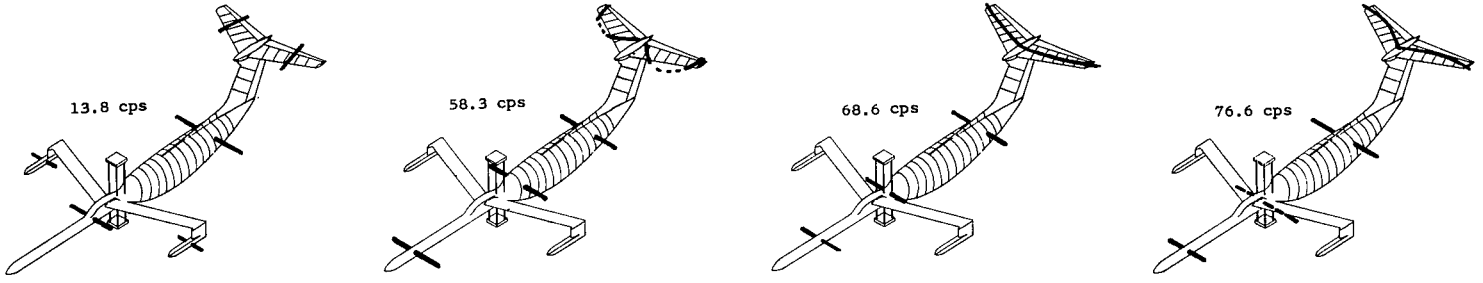

(a) Symmetric modes.

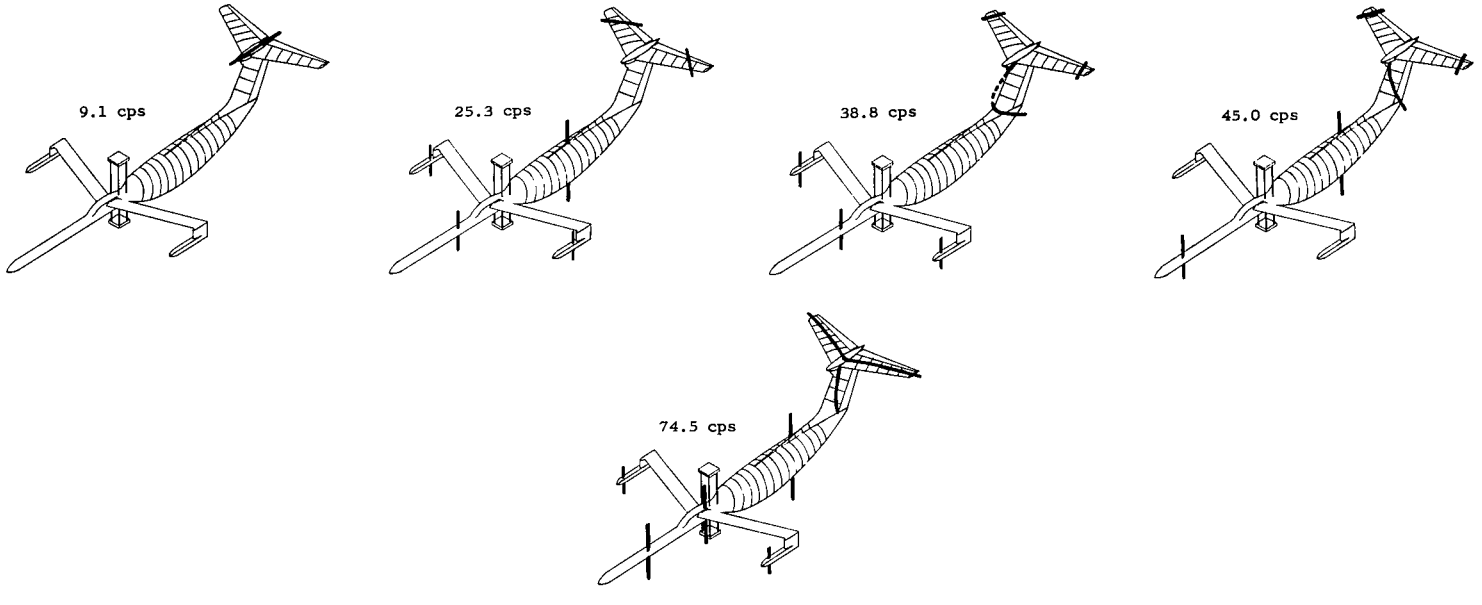

(b) Antisymmetric modes.

Figure 5.- Measured node lines associated with natural vibration frequencies for configuration B1-38.

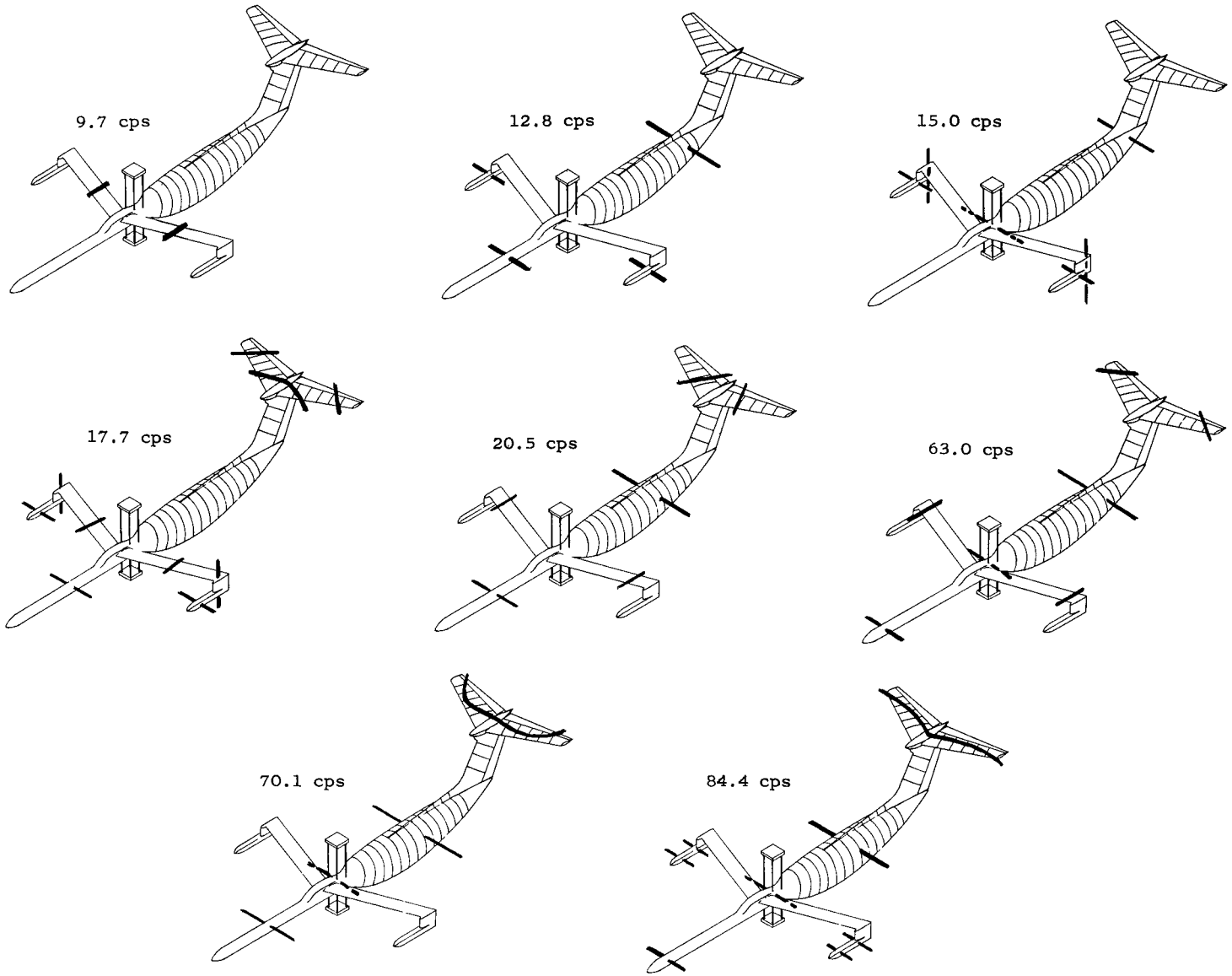

(a) Symmetric modes.

Figure 6.- Measured node lines associated with natural vibration frequencies for configuration C1-0.

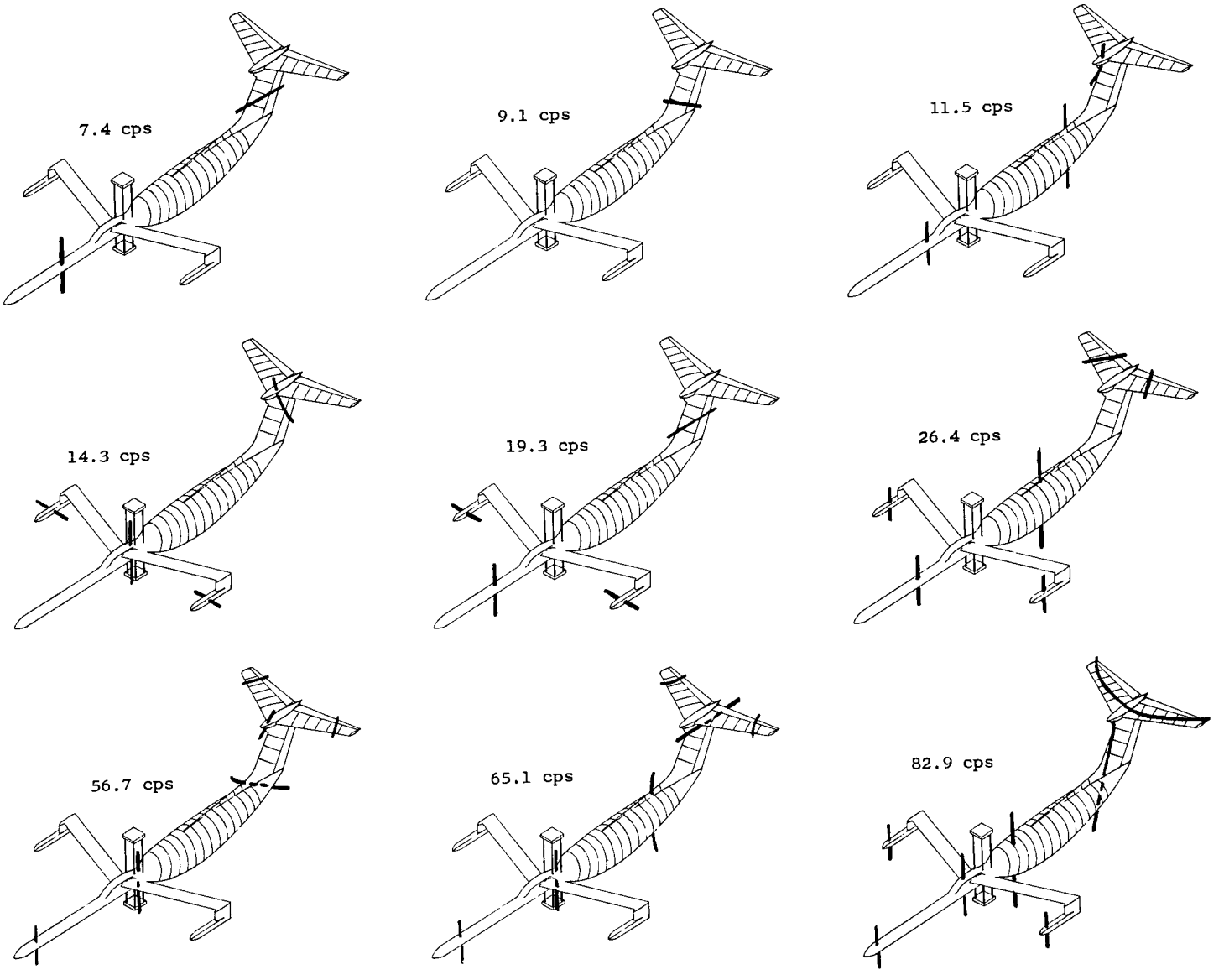

(b) Antisymmetric modes.

Figure 6.- Concluded.

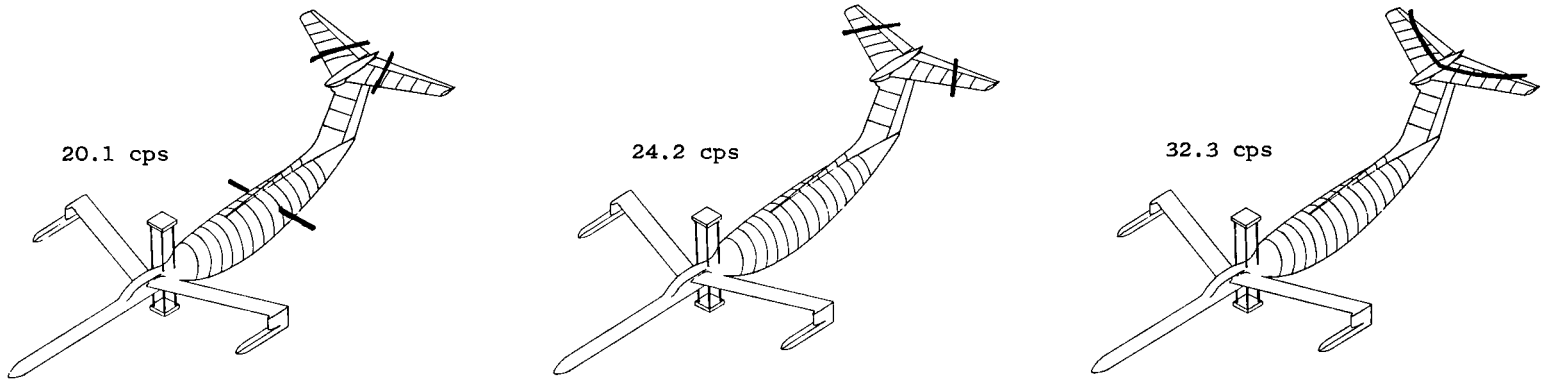

(a) Configuration C3-0.

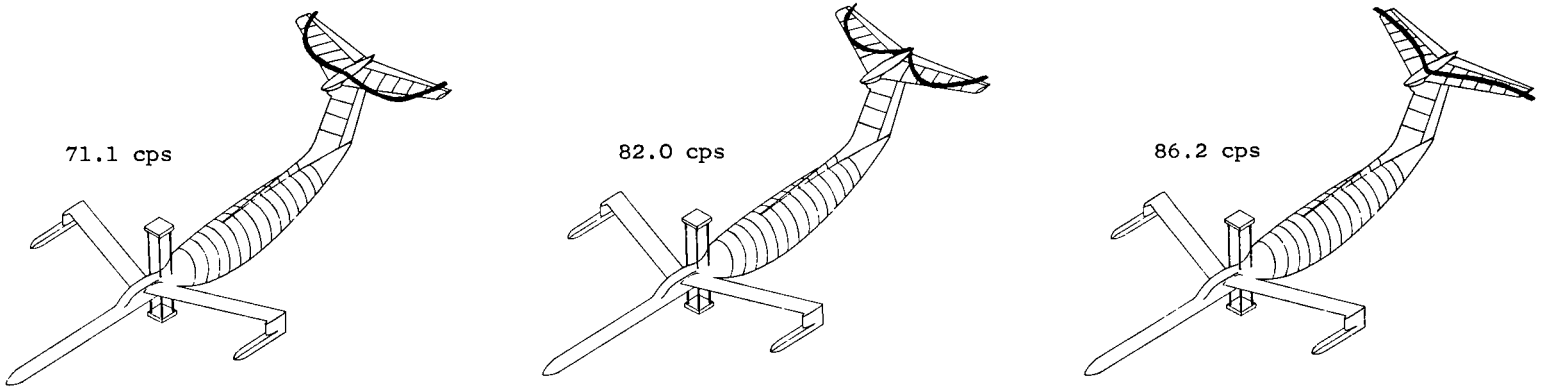

(b) Configuration C4-0.

Figure 7.- Measured node lines associated with symmetric natural vibration frequencies for configurations C3-0 and C4-0.

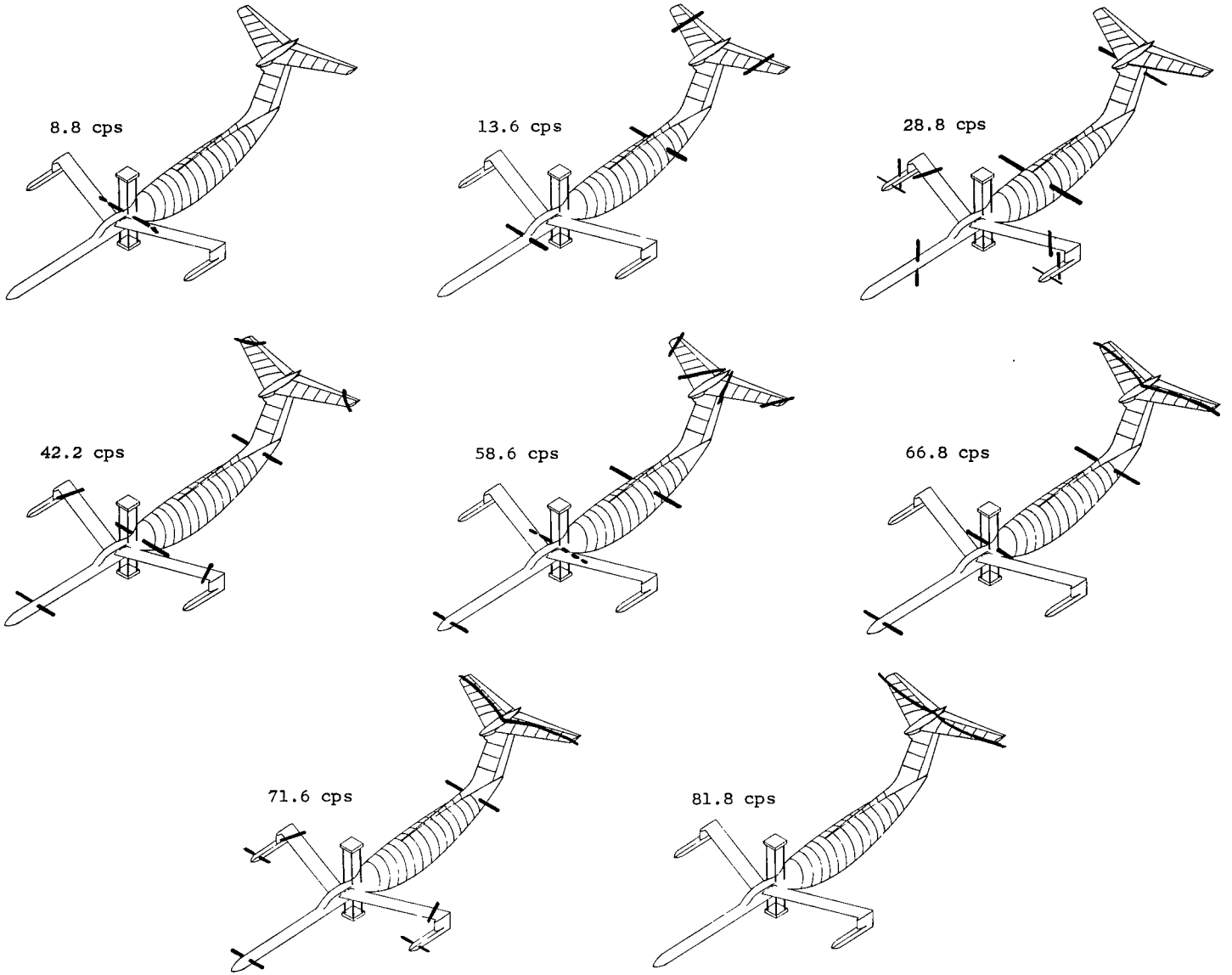

(a) Symmetric modes.

Figure 8.- Measured node lines associated with natural vibration frequencies for configuration C4-48s.

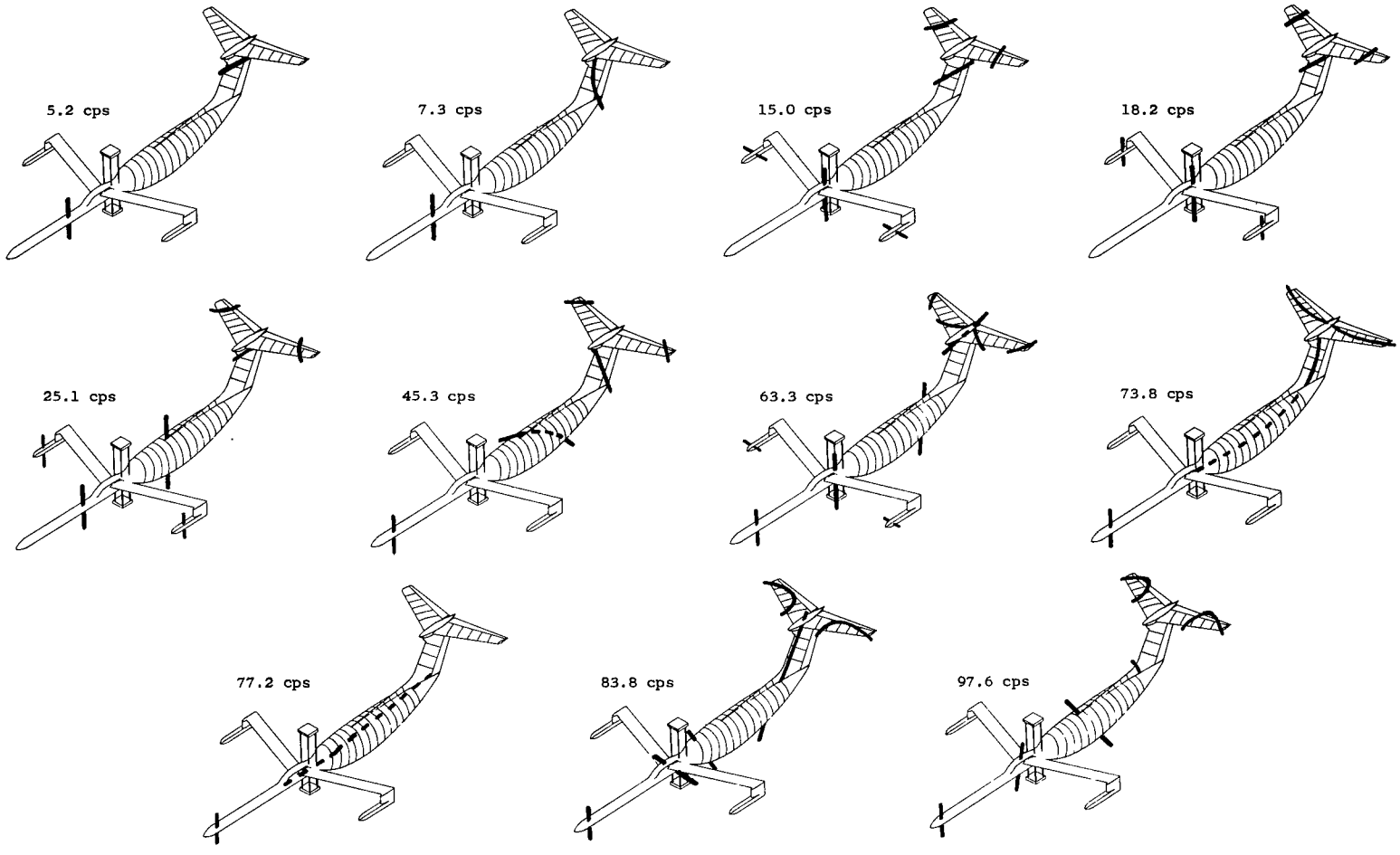

(b) Antisymmetric modes measured with drag cables mounted at wing midsemispan.

Figure 8.- Continued.

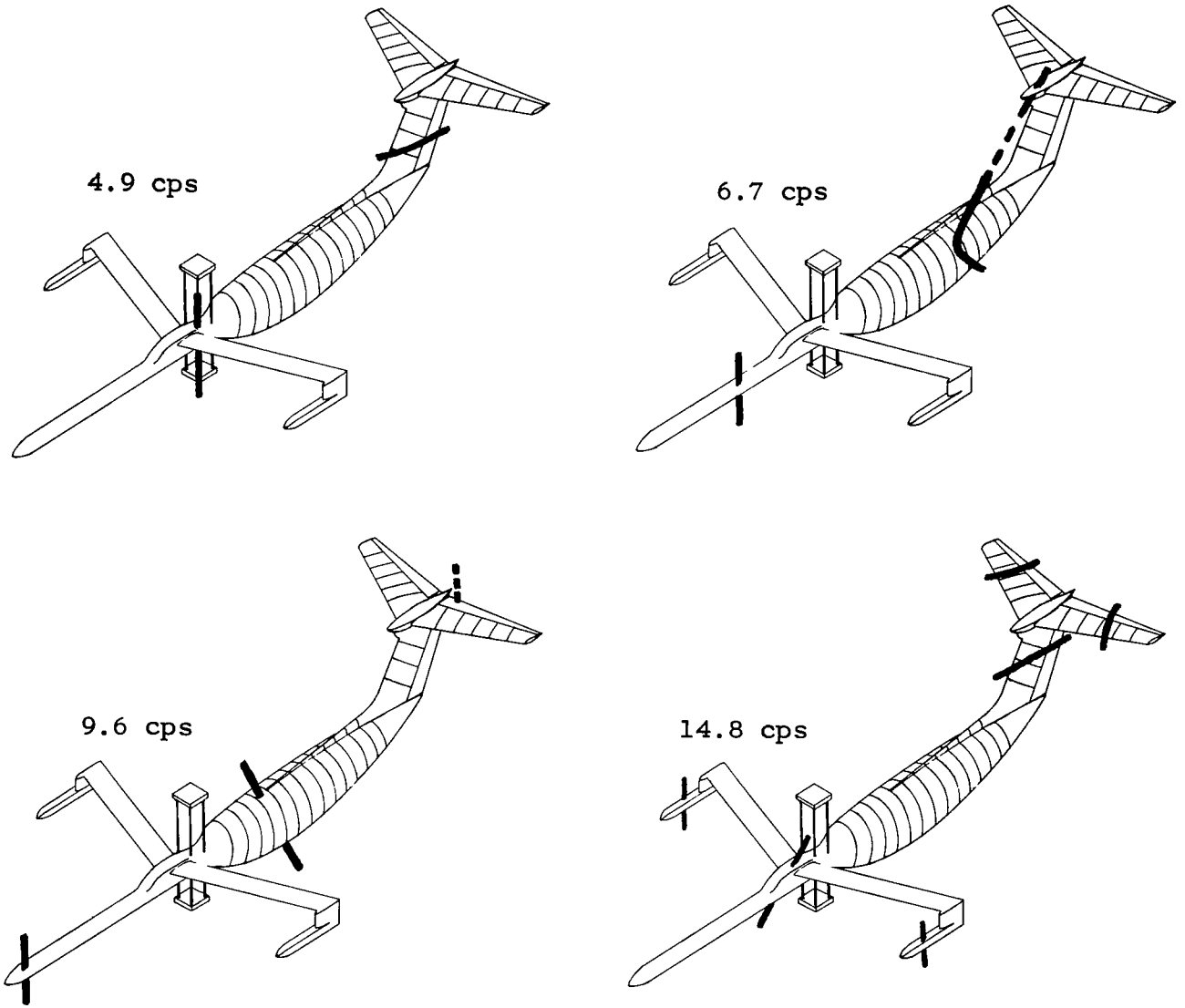

(c) Antisymmetric modes measured with drag cables mounted to forward fuselage midsection.

Figure 8.- Concluded.

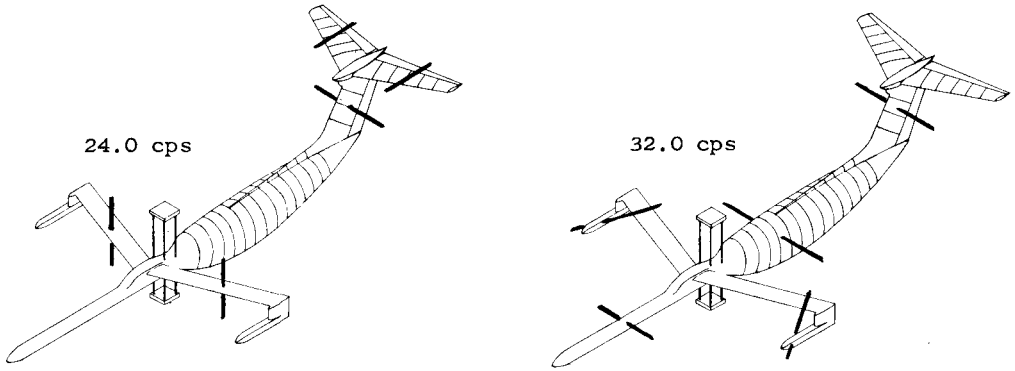

(a) Symmetric modes.

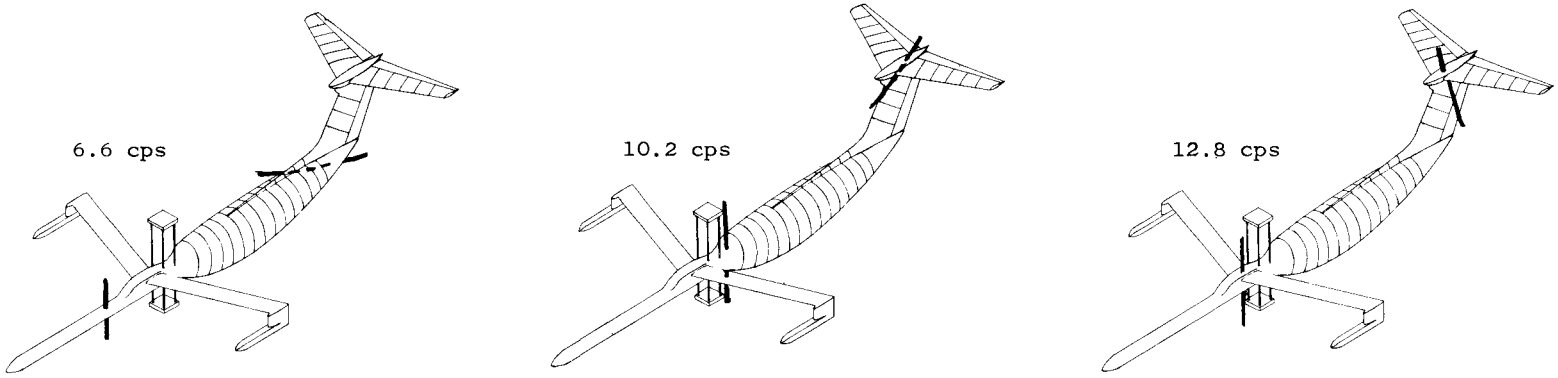

(b) Antisymmetric modes.

Figure 9.- Measured node lines associated with natural vibration frequencies for configuration D1-0.

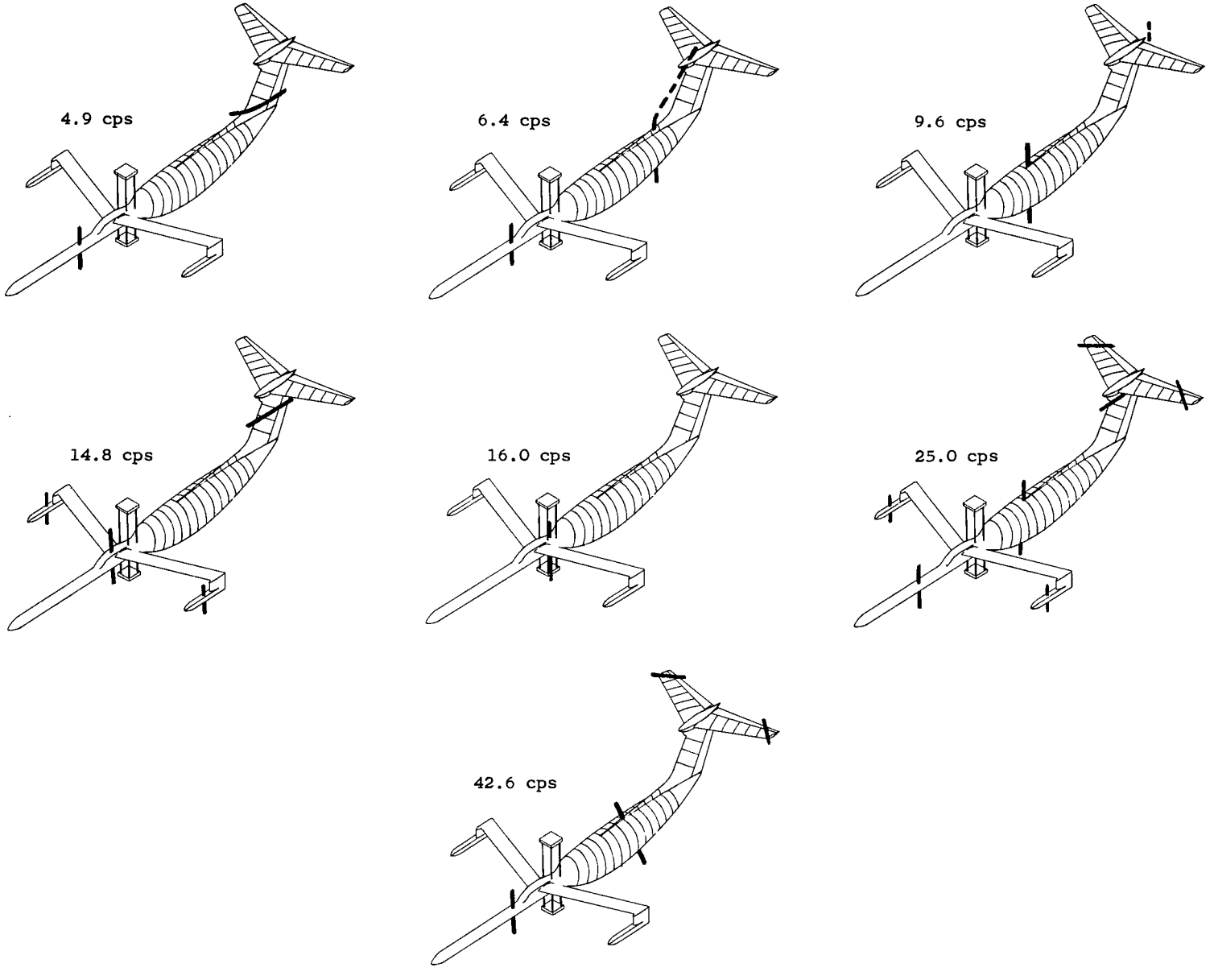

Figure 10.- Measured node lines associated with antisymmetric natural frequencies for configuration D4-48s.

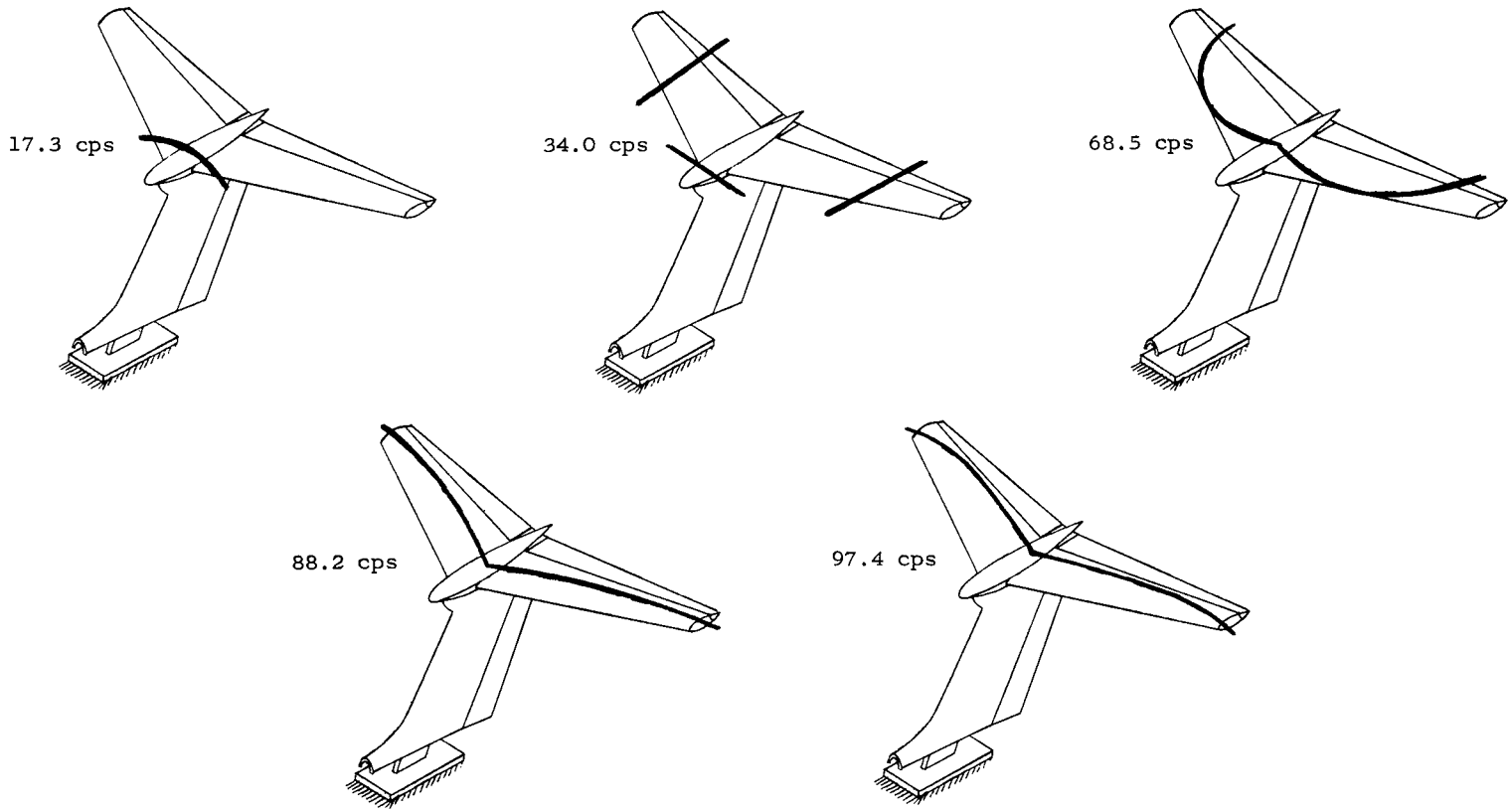

(a) Symmetric modes.

Figure 11.- Measured node lines associated with natural vibration frequencies for empennage of configuration C1-0 cantilevered at the fin root.

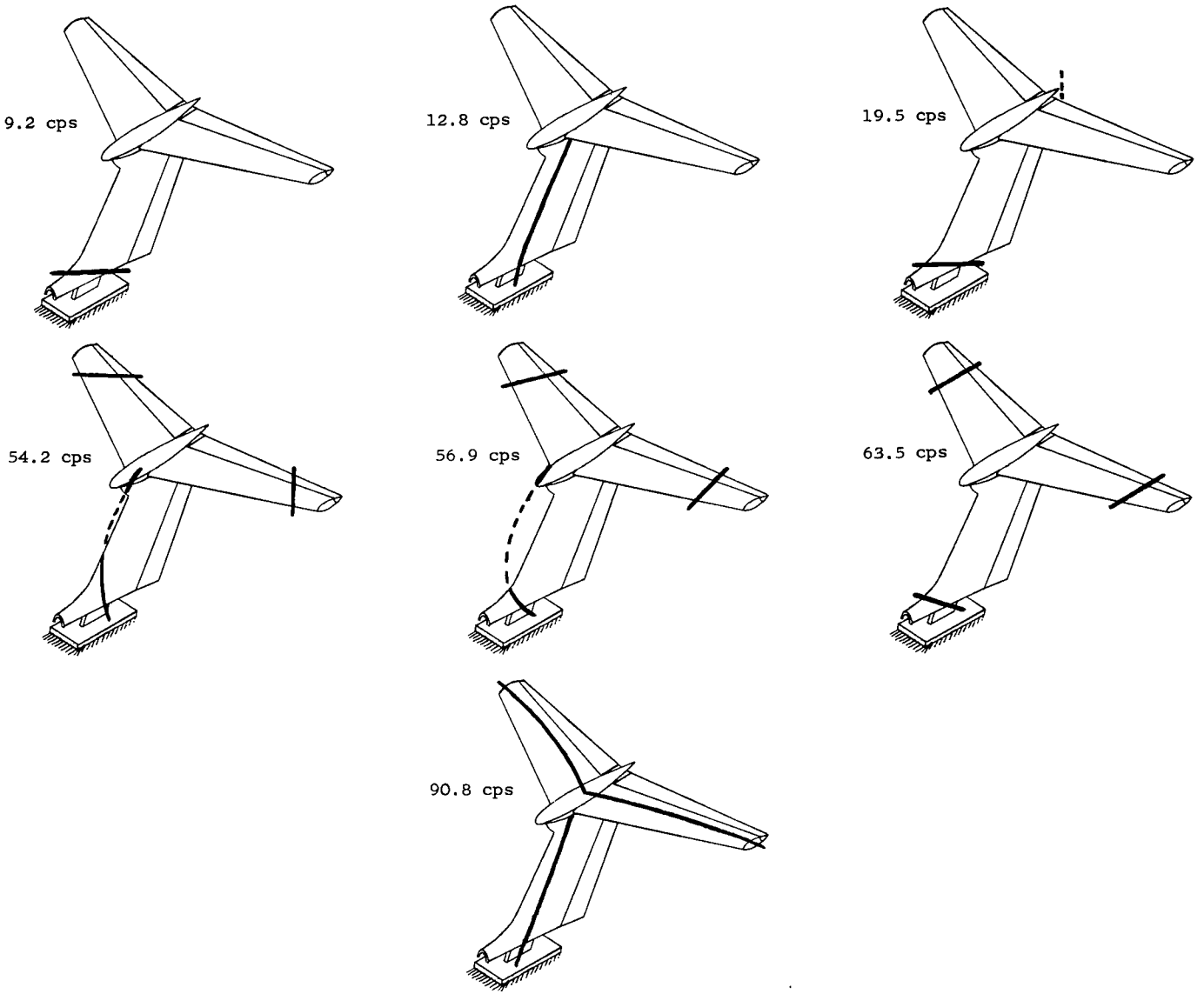

(b) Antisymmetric modes.

Figure 11.- Concluded.

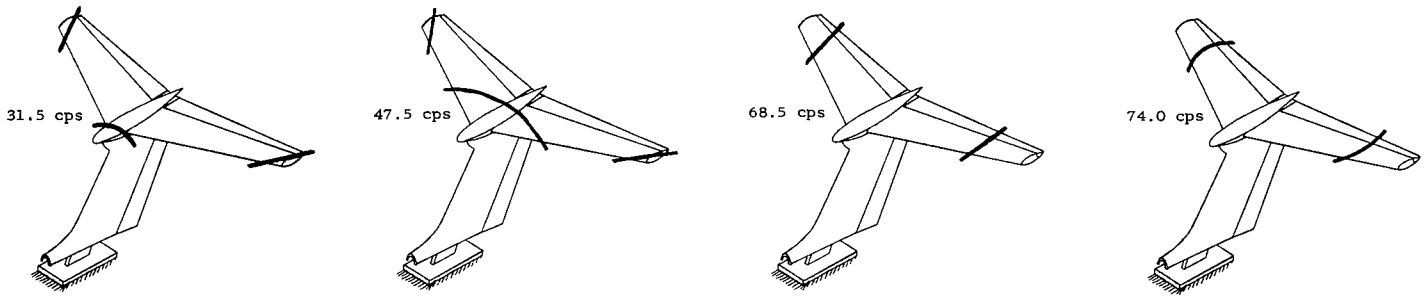

(a) Configuration C2-0.

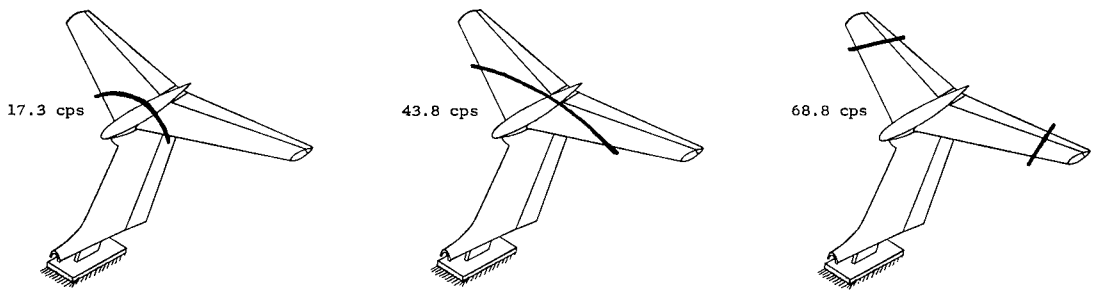

(b) Configuration C3-0.

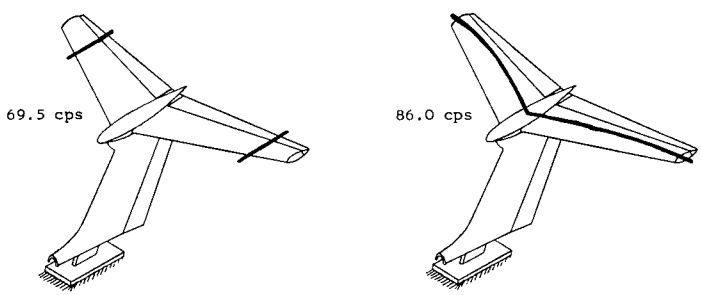

(c) Configuration C4-0.

Figure 12.- Measured node lines associated with symmetric natural vibration frequencies for empennage of configurations C2-0, C3-0, and C4-0 cantilevered at fin root.

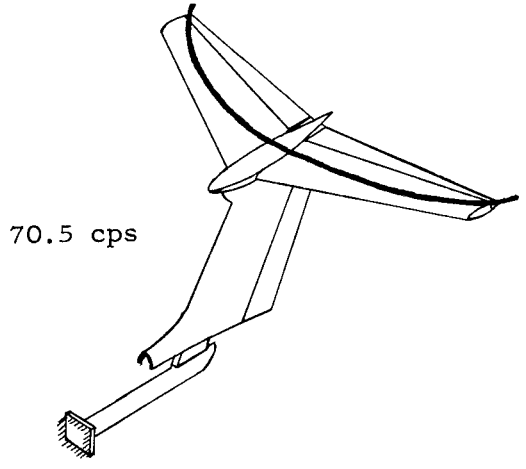

(a) Configuration E1-0s.

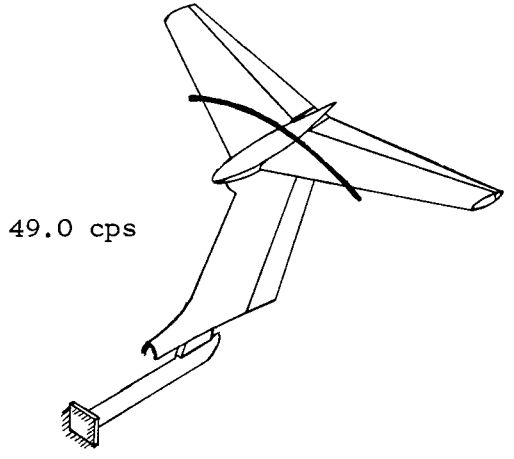

(b) Configuration E2-0s.

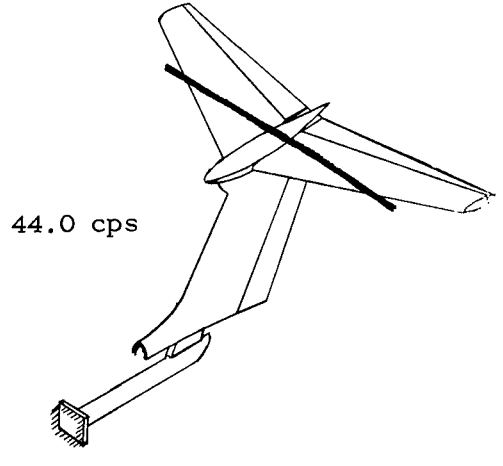

(c) Configuration E3-0s.

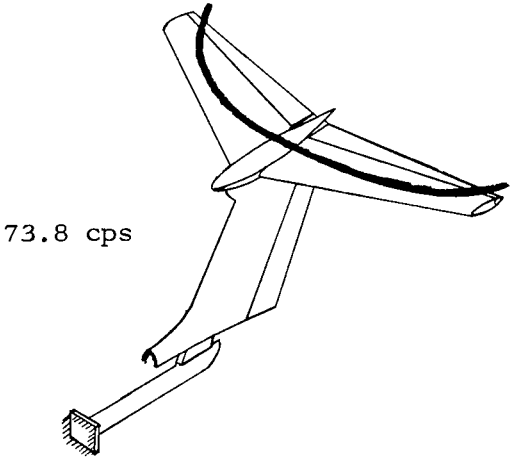

(d) Configuration E4-0s.

Figure 13.- Measured node lines associated with symmetric natural vibration frequencies for empennage of configurations E1-0s, E2-0s, E3-0s, and E4-0s cantilevered at FS 158.8.

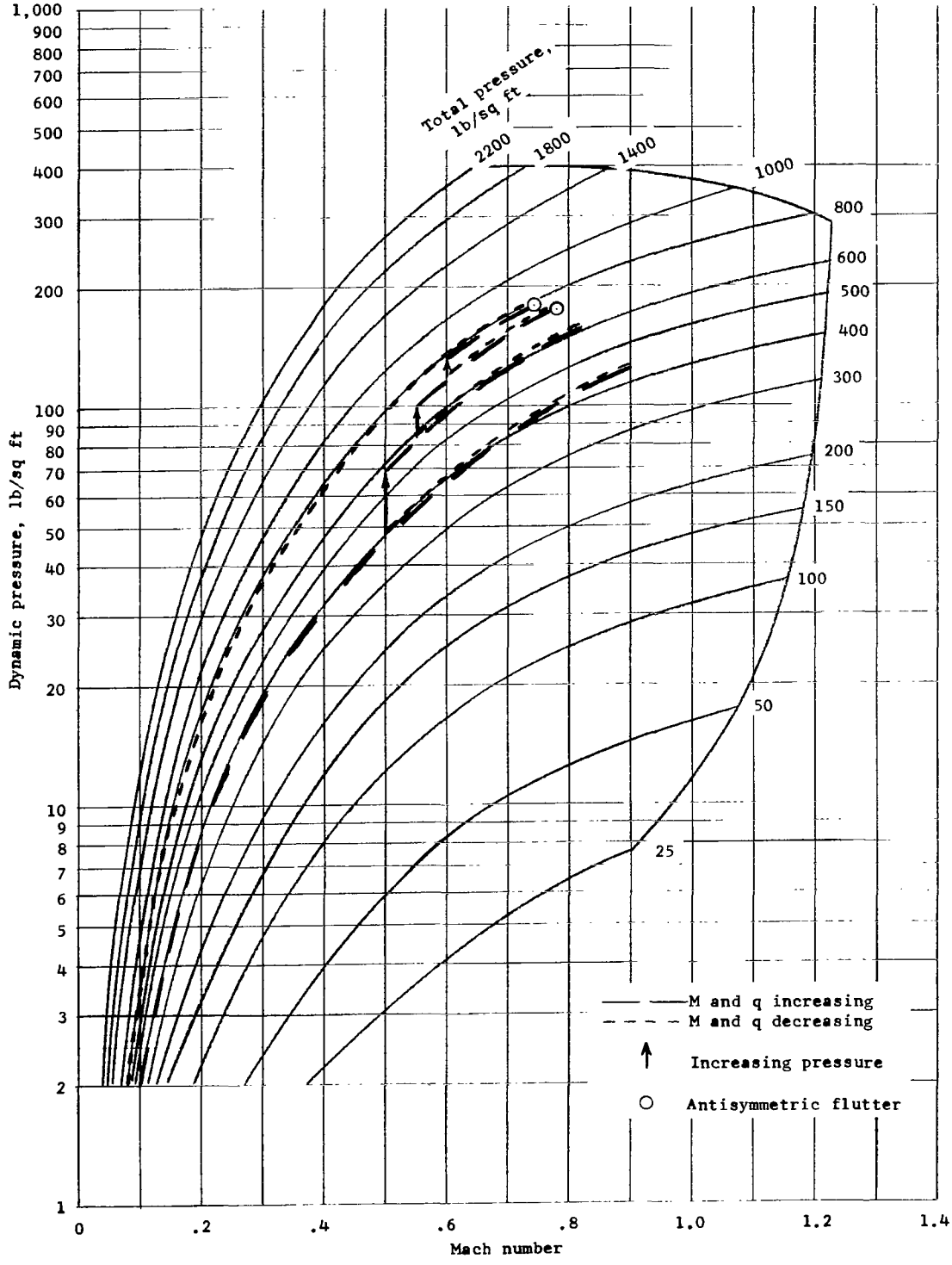

Figure 14.- Typical operating procedure for test in Freon-12.

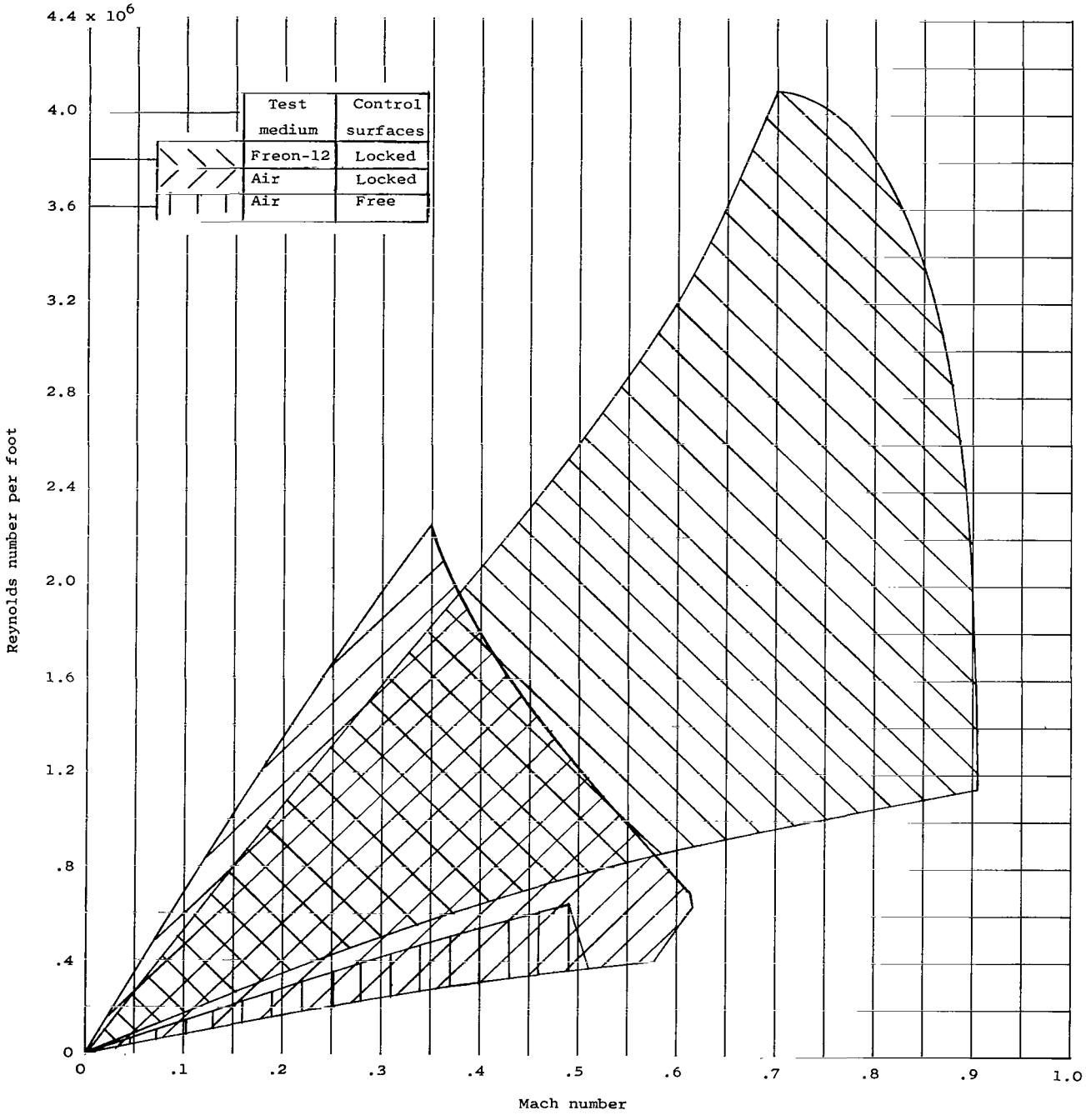

Figure 15.- Reynolds numbers and Mach numbers covered in the present investigation.

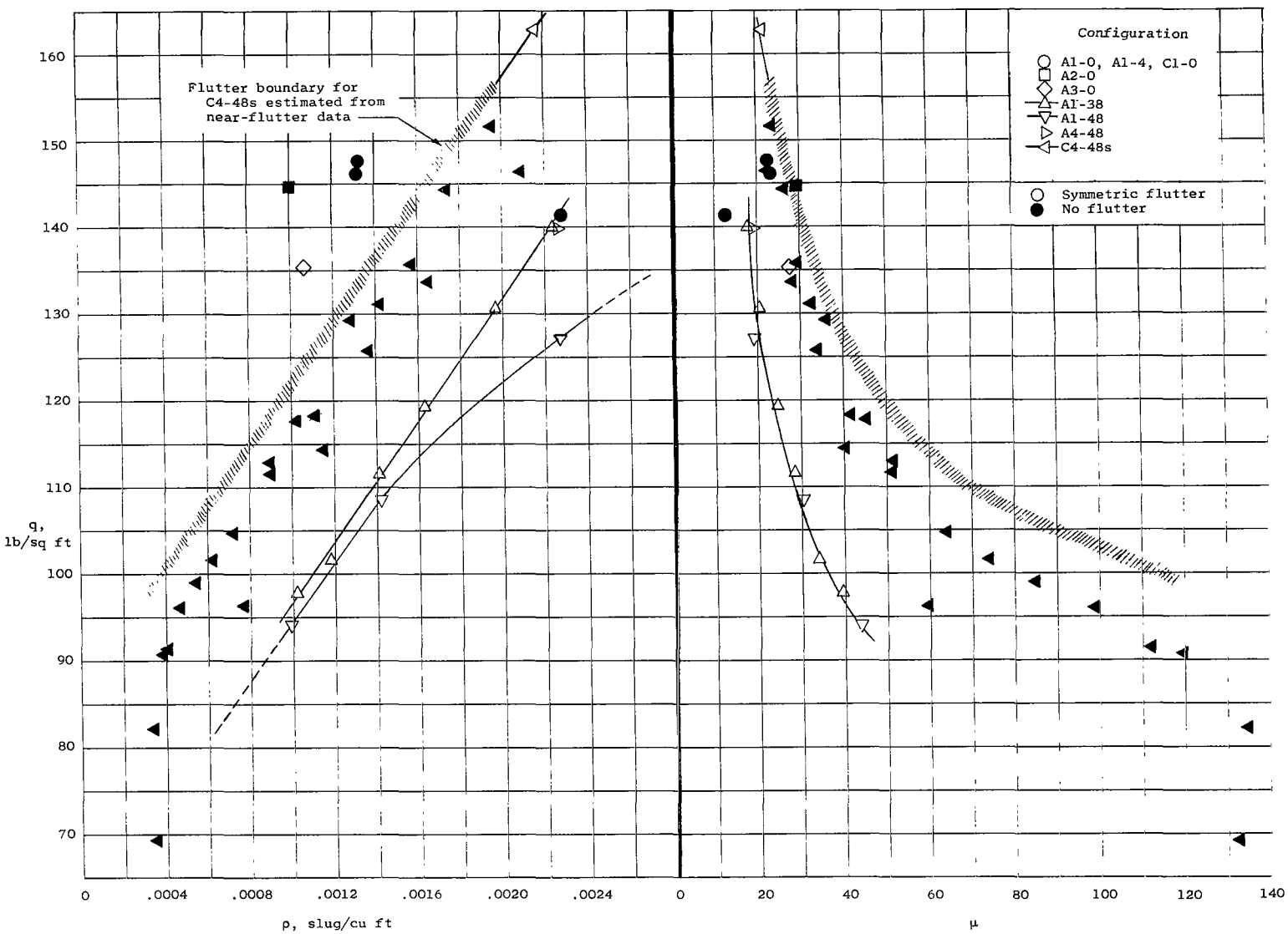

Figure 16.- Variation of dynamic pressure with air density and with mass ratio for configurations tested in air with control surfaces locked. $M < 0.62$.

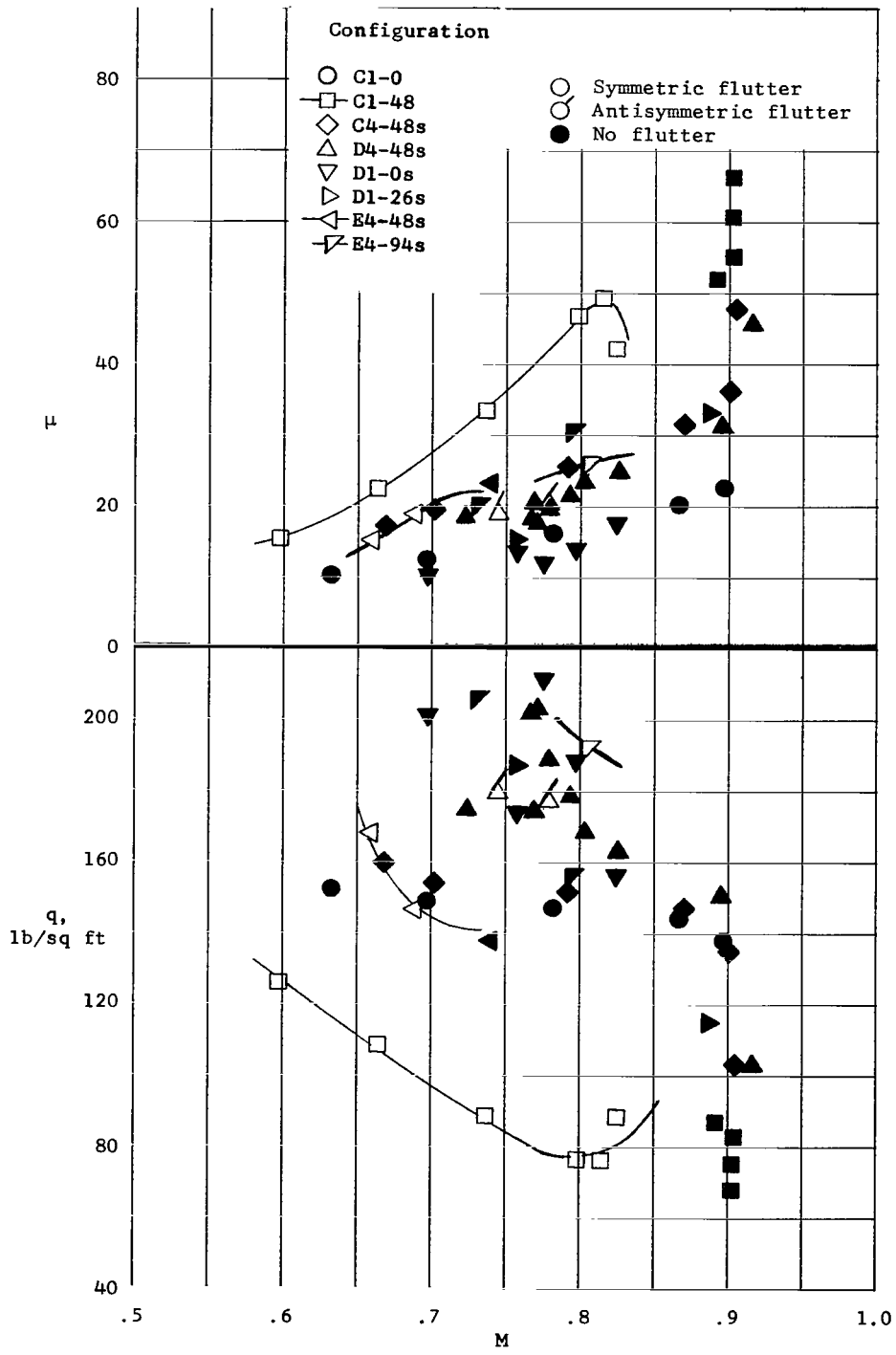

Figure 17.- Variation of dynamic pressure and mass ratio with Mach number for configurations tested in Freon-12 with control surfaces locked.

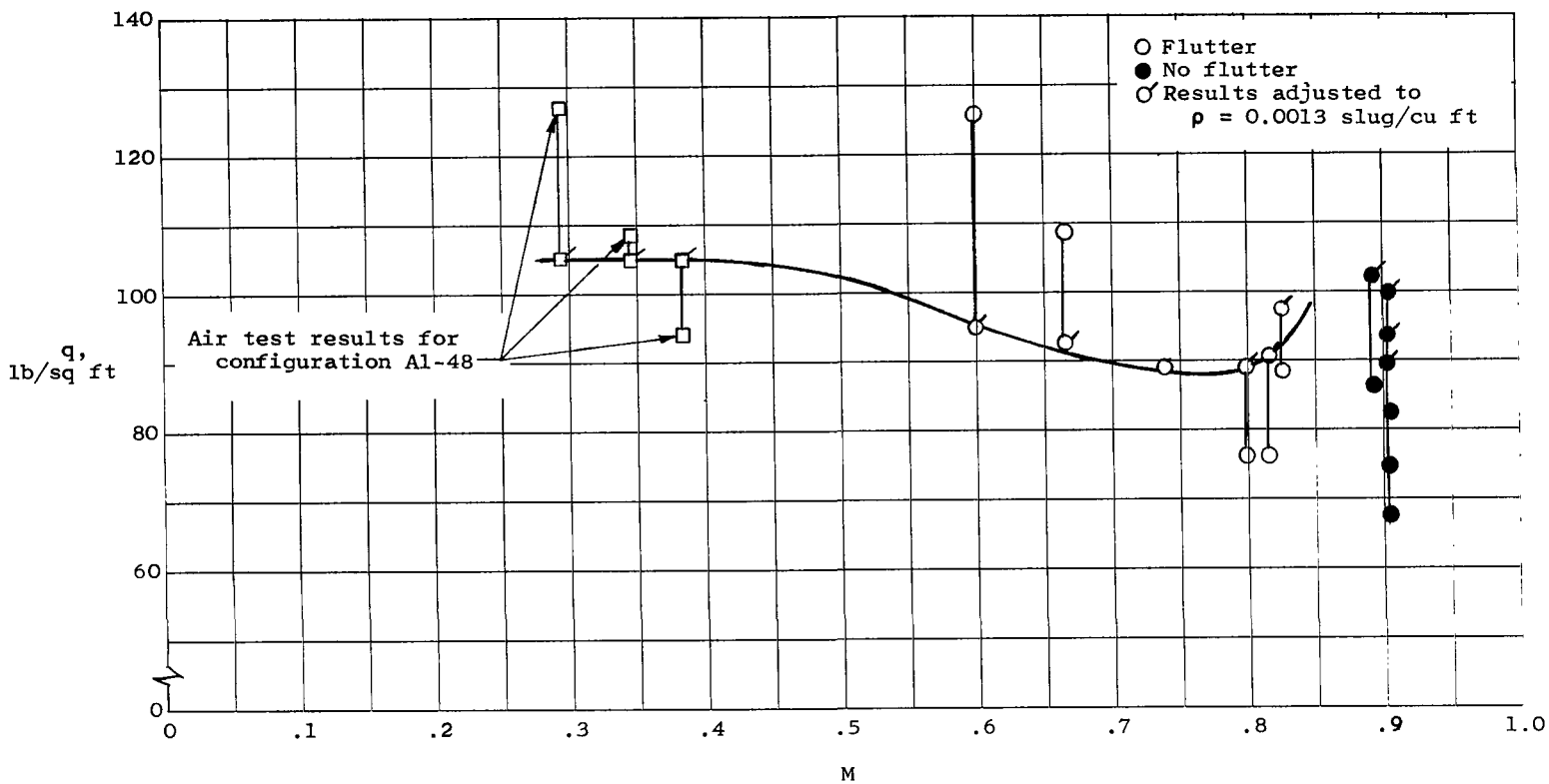

Figure 18.- Variation with Mach number of the dynamic pressure adjusted to a constant density for configuration C1-48.

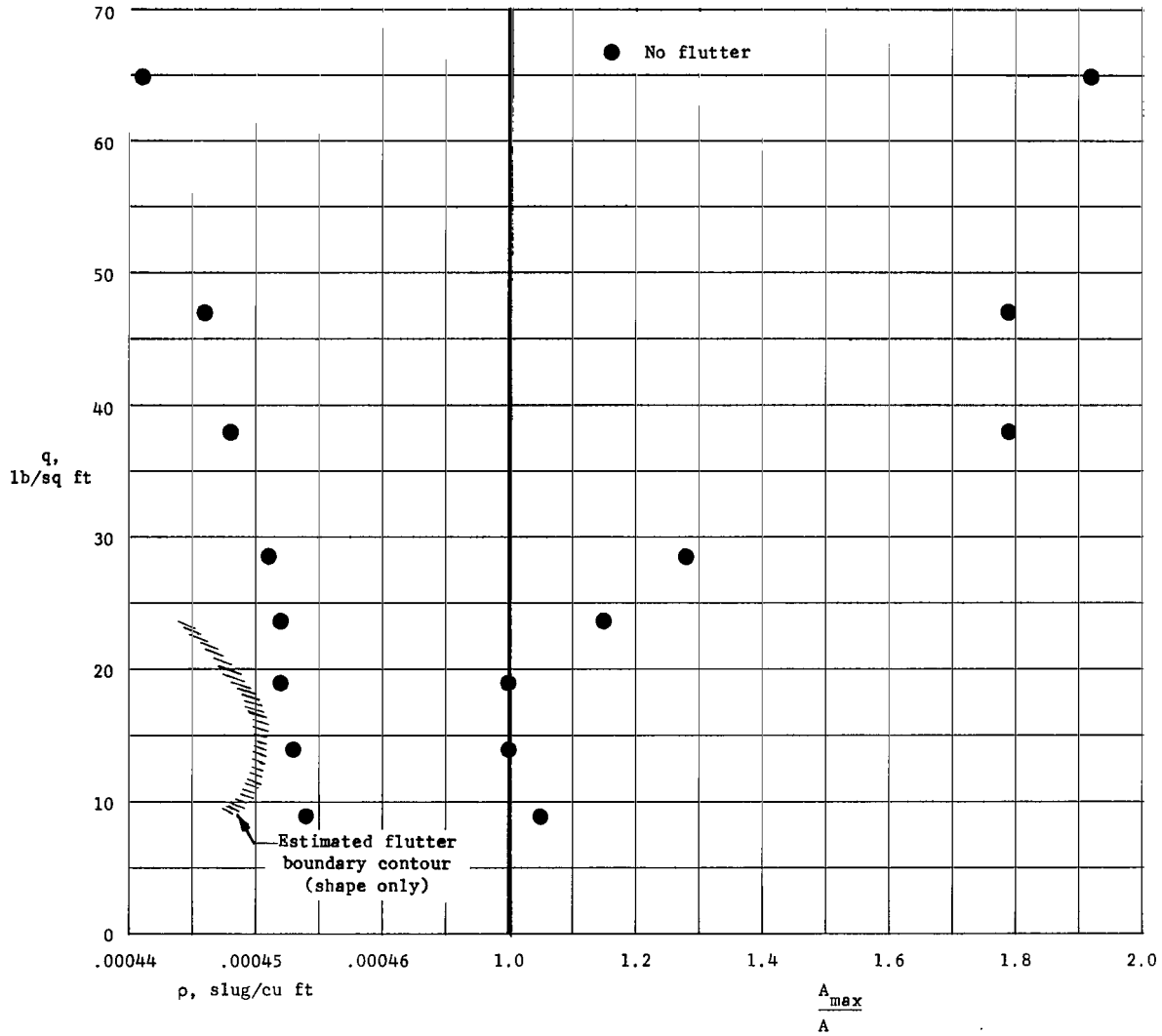

(a) Variation of dynamic pressure with air density.

(b) Variation of dynamic pressure with normalized inverse amplitude of rudder rotation.

Figure 19.- Results obtained in air for configuration B1-0 with rudder free to rotate on flexures. $M < 0.50$.

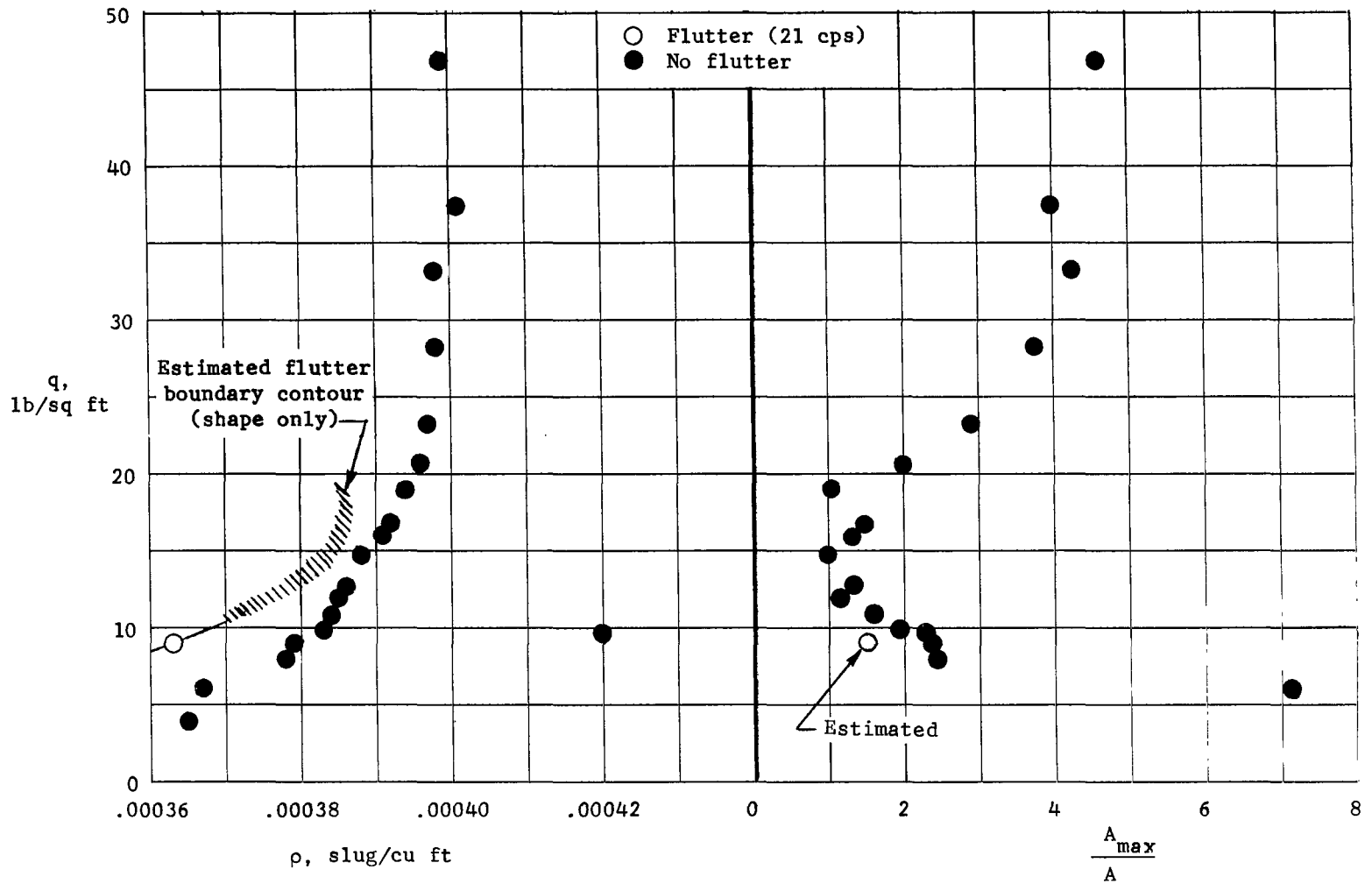

(a) Variation of dynamic pressure with air density.

(b) Variation of dynamic pressure with normalized inverse amplitude of elevator rotation.

Figure 20.- Results obtained in air for configuration B1-0 with elevators free to rotate on flexures. $M < 0.44$.

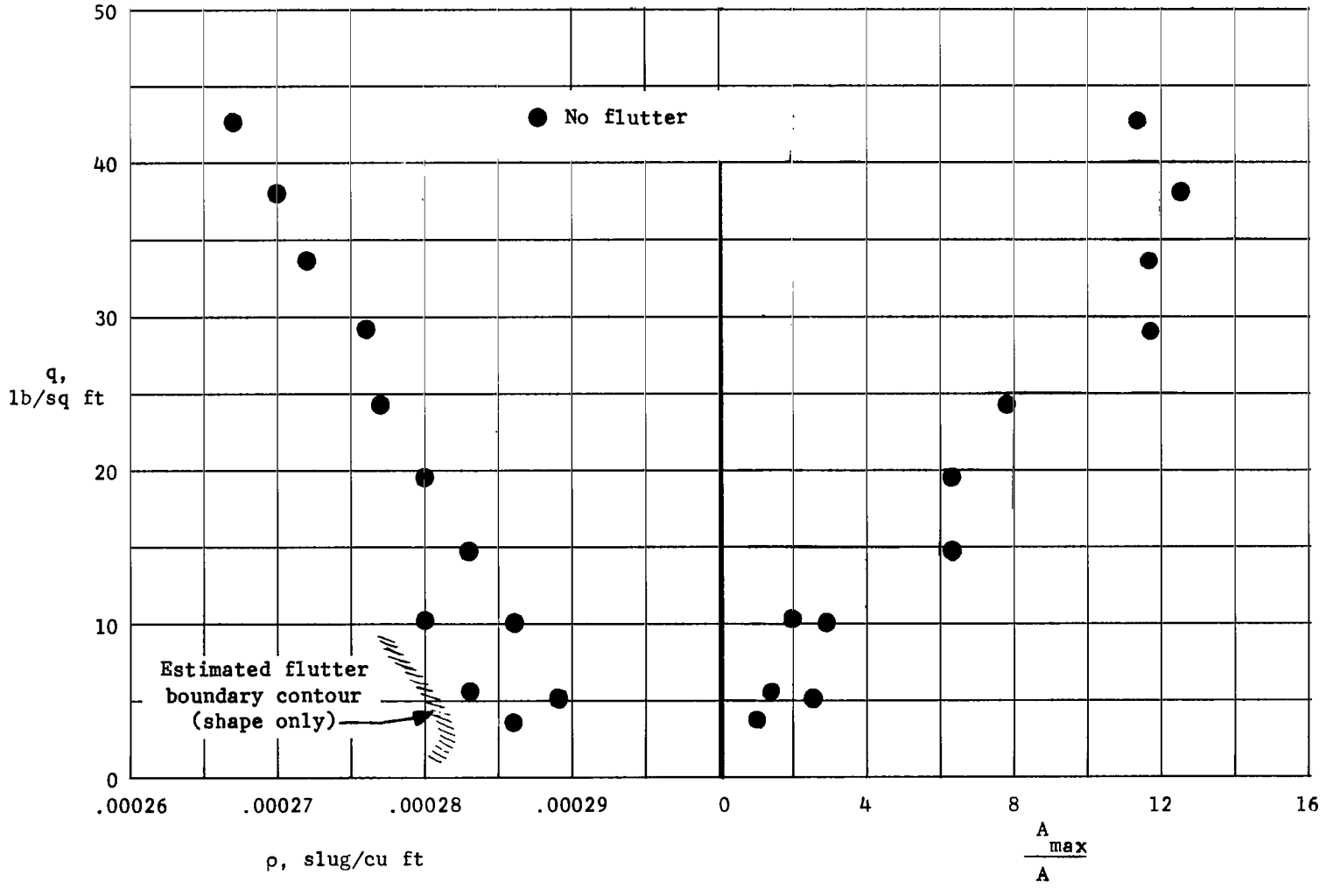

(a) Variation of dynamic pressure with air density.

(b) Variation of dynamic pressure with normalized inverse amplitude of elevator rotation.

Figure 21.- Results obtained in air for configuration C1-0 with simulated design symmetric rotational stiffness of the elevators but with greater-than-design antisymmetric rotational stiffness. $M < 0.51$.